

RESEARCH ARTICLE

[View Article Online](#)
[View Journal](#)

Cite this: DOI: 10.1039/d5md00339c

5-(Thiophen-2-yl)isoxazoles as novel anti-breast cancer agents targeting ER α : synthesis, *in vitro* biological evaluation, *in silico* studies, and molecular dynamics simulation†

Paramita Pattanayak, ^a Sripathi Nikhitha, ^b Debojyoti Halder, ^b
Balamram Ghosh ^{*b} and Tanmay Chatterjee ^{*a}

Herein, we report the design and synthesis of novel 5-(thiophen-2-yl)-4-(trifluoromethyl)isoxazoles (TTI), and *in vitro* evaluation of their anti-cancer activities. Based on the molecular structure of our previously developed isoxazole-based anti-breast cancer lead molecule, 3-(3,4-dimethoxyphenyl)-5-(thiophen-2-yl)-4-(trifluoromethyl)isoxazole (TTI-4), we designed a set of 14 new analogues of TTI-4. The TTIs are a synthetically challenging class of molecules, and we synthesized them with high purity by utilizing our in-house developed novel synthetic strategy, *i.e.*, metal-free, cascade regio- and stereoselective trifluoromethyloximation, cyclization, and elimination strategy, with readily available α,β -unsaturated ketones by using commercially available and cheap reagents such as $\text{CF}_3\text{SO}_2\text{Na}$ and $^t\text{BuONO}$ (cost-effective and sustainable synthesis). Subsequently, the anti-cancer activities of the newly synthesized molecules were evaluated against various cancer cell lines such as MCF-7, 4T1, and PC-3, and the molecules showed potential and more selective cytotoxicity against the human breast cancer cell line, MCF-7, among others. The *in vitro* screening revealed a new molecule, *i.e.*, 5-(thiophen-2-yl)-4-(trifluoromethyl)-3-(3,4,5-trimethoxyphenyl)isoxazole (TTI-6), possessing an IC_{50} value of 1.91 μM against MCF-7, is superior to the previous lead molecule (TTI-4) and also the best anti-cancer agent among all. The structure–activity relationship (SAR) studies revealed the importance of an unsubstituted thiophene ring in the 5th position, a $-\text{CF}_3$ functional group in the 4th position, and a highly electron-rich benzene ring bearing three $-\text{OCH}_3$ functional groups in the 3rd position of the isoxazole core to have superior activity. Further studies with TTI-6, such as apoptosis induction, cell cycle analysis, and nuclear staining, revealed an apoptotic cell death mechanism. The *in silico* molecular docking, induced fit analysis, and ADMET studies further supported the effects of various functional groups of TTIs on their anti-breast cancer activity by inhibiting the estrogen receptor alpha (ER α), a crucial nuclear hormone receptor involved in gene regulation that plays an important role in several human cancers.

Received 19th April 2025,
Accepted 24th June 2025

DOI: 10.1039/d5md00339c

rsc.li/medchem

Introduction

Cancer is a complex and life-threatening disease characterized by uncontrolled cell growth, invasion, and metastasis.^{1,2} It

arises due to genetic and epigenetic alterations that disrupt normal cell cycle regulation, leading to tumor formation and progression.^{3–6} Among various types of cancers, breast cancer is the most frequently diagnosed cancer and one of the leading causes of cancer-related deaths among women worldwide. Among all types of breast cancers, such as hormone receptor-positive breast cancer, HER2-positive breast cancer, triple-negative breast cancer (TNBC), inflammatory breast cancer (IBC), and metaplastic breast cancer, ER-positive breast cancer (which expresses estrogen receptor alpha, ER α) accounts for approximately 70–75% of all breast cancer cases and is primarily driven by estrogen signaling.^{7–9}

ER α is a nuclear hormone receptor that is involved in regulating gene expression. It plays a critical role in breast cancer pathogenesis by regulating gene expression involved

^a Department of Chemistry, Birla Institute of Technology and Science, Pilani (BITS Pilani), Hyderabad Campus, Jawahar Nagar, Hyderabad 500078, Telangana, India. E-mail: tanmay@hyderabad.bits-pilani.ac.in

^b Epigenetic Research Laboratory, Department of Pharmacy, Birla Institute of Technology and Science, Pilani (BITS Pilani), Hyderabad Campus, Jawahar Nagar, Hyderabad 500078, Telangana, India.

E-mail: balaram@hyderabad.bits-pilani.ac.in

† Electronic supplementary information (ESI) available: Analytical data, ^1H , ^{19}F and ^{13}C NMR spectra, HRMS spectra of all the synthesised compounds, molecular docking analysis data, HPLC spectra of the lead molecule TTI-6. See DOI: <https://doi.org/10.1039/d5md00339c>



in cell proliferation, differentiation, and survival. It gets activated when it binds to estrogen, especially 17 β -estradiol. The activation of ER α results in conformational changes, dimerization, and translocation to the nucleus, where it attaches itself to target gene promoter regions' estrogen response elements (EREs). This binding initiates transcriptional programs that direct the proliferation of breast epithelial cells.¹⁰ Hence, ER α is a crucial target in breast cancer therapy. The crystal structure of ER α (PDB: 3ERT) revealed the ligand-binding domain of ER α with 4-hydroxy tamoxifen (4HT), a selective estrogen receptor modulator. A pharmacophore is a set of molecular features essential for optimal interactions with a particular pharmacological target. The essential pharmacophoric features in the ER α (PDB: 3ERT) complex include hydrophobic interactions. The hydrophobic nature of the ER α ligand-binding domain (LBD) is significant for the accommodation of 4HT, a hydrophobic molecule. The non-polar aromatic rings of 4HT, comprising three interconnected aromatic rings, showed crucial hydrophobic interactions at the catalytic binding pocket of ER α . These rings interact with the hydrophobic residues of the binding pocket, primarily leucine amino acid residues (LEU346, LEU384, and LEU387), *via* van der Waals interactions. The ethyl side chain of tamoxifen interacts with residues of PHE404 and LEU391, which contribute to the stabilization. These hydrophobic interactions are extremely crucial for the positioning of inhibitors like 4HT in a way that disrupts the usual activation function of ER α and exerts an antagonistic effect. The other pharmacophoric features include the hydrogen-bond donor or acceptor ability of the hydroxyl group (-OH) present at the *para*-position of one of the benzene rings of the 4HT, which forms a hydrogen bond with glutamic acid (GLU353) and

arginine (ARG394) in the ligand-binding domain. The interconnected aromatic moieties of 4HT are essential for fitting into the catalytic binding site of the hydrophobic cavity of the target. This aromatic ring system and the bulky nature of the ethyl side chain introduce a displacement of helix 12. It adopts a position that obstructs the coactivator binding groove, and this structural alteration is a hallmark of antagonistic modulation, rendering ER α transcriptionally inactive. The overall dipole moment generated by the aromatic moieties enhances interaction stability at the inhibitor binding pocket. These are the essential pharmacophores needed for the inhibitor activity at the ER α complex for anti-breast cancer therapeutics.¹¹

Current treatments for ER α -positive breast cancer include FDA-approved drugs tamoxifen, fulvestrant, and letrozole, which help to block estrogen binding, promote ER α degradation, and reduce estrogen production, respectively (Fig. 1a).¹⁰ However, drug resistance and recurrence remain significant obstacles in ER α -targeted therapy, highlighting the need for novel small-molecule inhibitors with enhanced efficacy and selectivity.

The isoxazole core, an important pharmacophore in drug design, is a crucial heterocyclic scaffold in medicinal chemistry due to its unique electronic properties and structural stability.^{12–14} Isoxazole-based drugs play a vital role in medicinal chemistry due to their broad-spectrum biological activities, including anti-inflammatory, anticancer, antimicrobial, and anticonvulsant properties. Notable examples include oxacillin (a β -lactam antibiotic), leflunomide (an immunosuppressant for rheumatoid arthritis), and valdecoxib (an anti-inflammatory) (Fig. 1b).¹⁵ Its electron-rich nature and heterocyclic framework contribute to strong interactions with enzymes and receptors, improving drug efficacy and selectivity.¹⁶

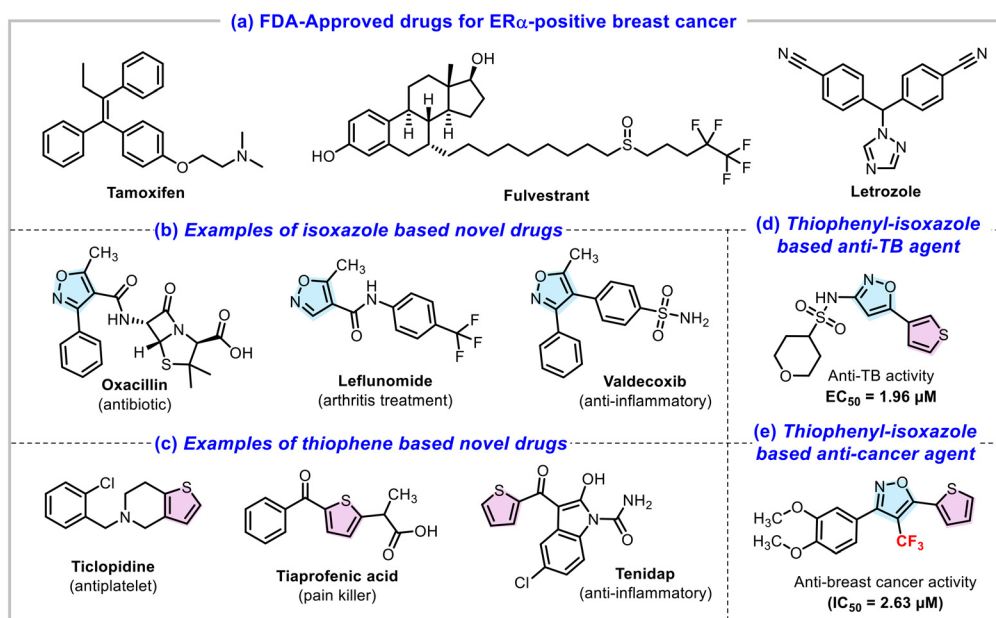


Fig. 1 (a) FDA-approved drugs for ER α -positive breast cancer, (b) some examples of isoxazole novel drugs, (c) some examples of thiophene-based drugs, (d) example of thiophenyl-isoxazole-based drug (A) and (e) our previously synthesised anti-breast cancer molecule (TTI).



On the other hand, the thiophene ring, a sulfur-containing five-membered aromatic ring, is another crucial heterocyclic moiety in drug design due to its aromatic stability, lipophilicity, and electronic properties, which enhance drug solubility, bioavailability, and metabolic stability.¹⁷ Thiophene-containing compounds exhibit diverse biological activities, including anticancer, anti-inflammatory, antimicrobial, and antidiabetic effects.^{18,19} Well-known drugs featuring thiophene rings include ticlopidine (antiplatelet), tiaprofenic acid (pain killer), and tenidap (anti-inflammatory) (Fig. 1c). Due to its versatile nature, thiophene continues to be widely explored in the development of new therapeutic agents. Although isoxazole- and thiophene-based drug molecules are well-known in the literature independently, thiophenyl-isoxazole-based compounds are less explored in medicinal chemistry. Yang *et al.* designed and synthesized several thiophenyl-isoxazole-based compounds to investigate anti-TB activity against *Mycobacterium tuberculosis*, and the most active one was found to have an EC₅₀ value of 1.96 μ M

(Fig. 1d).²⁰ Last year, our group designed and synthesized a series of novel 4-(trifluoromethyl)isoxazole-based molecules and evaluated their anti-cancer activity against MCF-7, 4T1, and PC-3 cancer cell lines.²¹ Interestingly, from the SAR studies, we found that isoxazole-bearing a thiophene ring at the 5th position, *i.e.*, 5-(thiophen-2-yl)isoxazole, exhibited the best IC₅₀ value against the MCF-7 cell line than those isoxazoles bearing a phenyl, furanyl, or vinyl functional group on its 5th position. Particularly, 3-(3,4-dimethoxyphenyl)-5-(thiophen-2-yl)-4-(trifluoromethyl)isoxazole **TTI-4** (IC₅₀ = 2.63 μ M) exhibited the best anti-cancer activity against the human breast cancer cell lines (MCF-7) (Fig. 1e and 2a).²¹

Being inspired by our previous studies, SAR analysis, and as a part of our continued interest in the discovery of new and novel anti-cancer molecules, we further designed a series of novel analogues of **TTI-4** (Fig. 2a), for the synthesis and evaluation of their cytotoxic activity against several cancer cell-lines including ER-positive breast cancer cell lines (MCF-7). Since it was evident from our previous studies that the presence of a trifluoromethyl

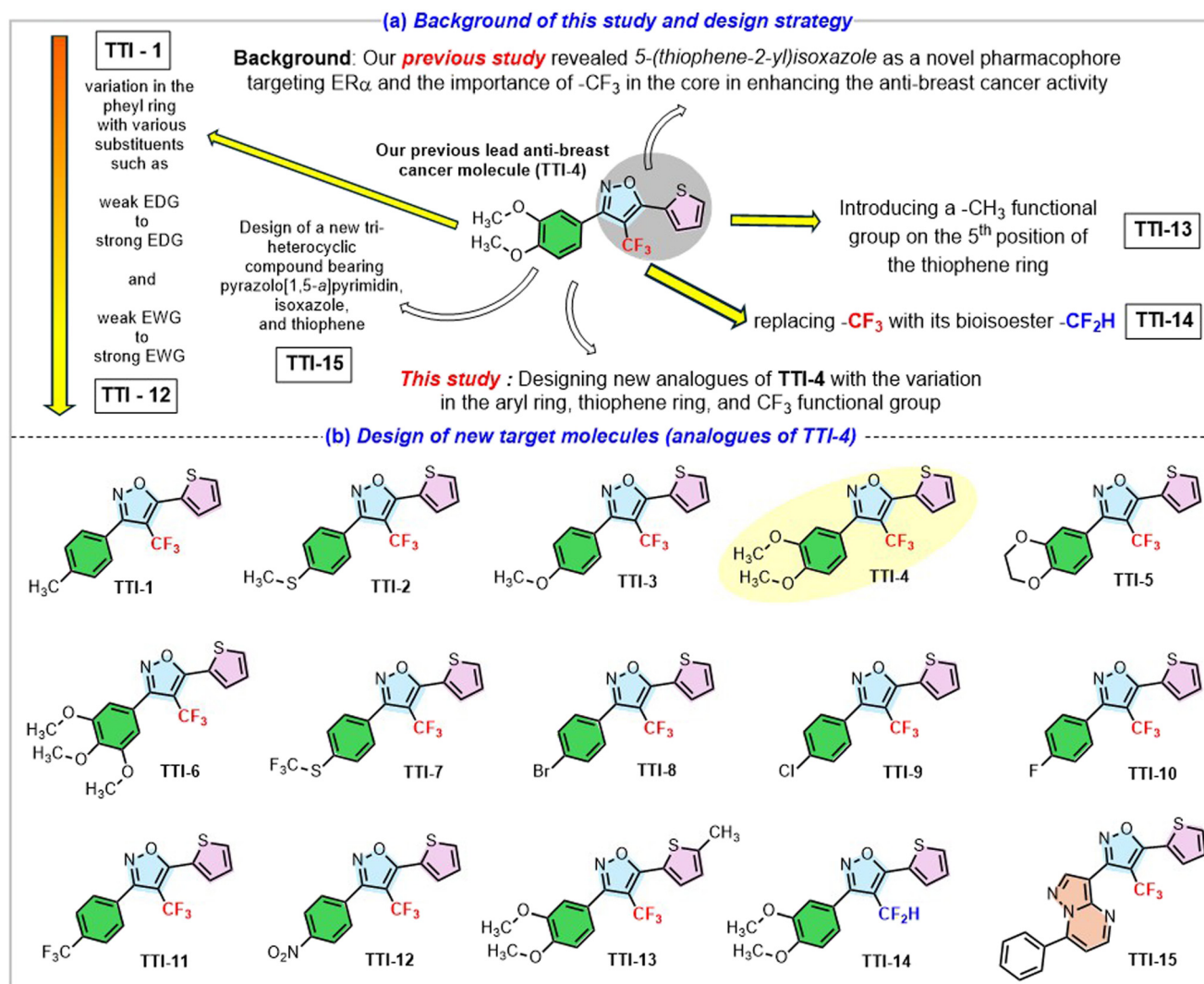


Fig. 2 (a) Background of this study and the design strategy, (b) molecular structure of the designed target molecules, *i.e.*, 5-(thiophene-2-yl)-isoxazoles (analogues of **TTI-4**) for synthesis and anti-cancer evaluation.



($-\text{CF}_3$) functional group in the 4th position of isoxazole enhances the anti-breast cancer activity to a significant extent, we decided to keep the $-\text{CF}_3$ functional group or its bioisoster, *i.e.*, $-\text{CF}_2\text{H}$ on the same position of isoxazole core. In particular, we designed a series of new 5-(thiophene-2-yl)isoxazoles bearing a CF_3 or CF_2H functional group on the 4th position (Fig. 2a). We primarily focused on the variation of the aryl functional group situated at the 3rd position of the isoxazole ring in our design strategy (Fig. 2a). Various electron-donating group ($4\text{-CH}_3\text{-C}_6\text{H}_4$ -, $4\text{-CH}_3\text{-S-C}_6\text{H}_4$ -, $4\text{-CH}_3\text{-O-C}_6\text{H}_4$ -, $3,4\text{-O-CH}_2\text{-CH}_2\text{-O-C}_6\text{H}_3$ -, $3,4,5\text{-tri-CH}_3\text{-O-C}_6\text{H}_2$ -, and $4\text{-CH}_3\text{-S-C}_6\text{H}_4$ -) substituted 5-(thiophen-2-yl)-4-(trifluoromethyl)-3-(aryl)isoxazoles (**TTI-1** to **TTI-3**, and **TTI-5** to **TTI-7**) were designed for the synthesis followed by anti-cancer evaluation to understand the effect of electron-releasing groups and various heteroatoms (O, S, and F) in the aryl ring on the anti-cancer activities in comparison to **TTI-4** (Fig. 2b). Next, to understand the effect of halogens, 5-(thiophen-2-yl)-4-(trifluoromethyl)-3-(aryl)isoxazoles bearing a halogen-substituted aryl ring ($4\text{-Br-C}_6\text{H}_4$ -, $4\text{-Cl-C}_6\text{H}_4$ -, and $4\text{-F-C}_6\text{H}_4$ -) were designed (**TTI-8** to **TTI-10**) (Fig. 2b). Since the presence of the $-\text{CF}_3$ functional group exhibited a great impact in enhancing the anti-cancer activity of isoxazoles, we designed another 5-(thiophen-2-yl)-4-(trifluoromethyl)-3-(aryl)isoxazole (**TTI-11**) bearing another $-\text{CF}_3$ functional group in the *para* position of the aryl ring (Fig. 2b). To know the effect of a strong electron-withdrawing group, 3-(4-nitrophenyl)-5-(thiophen-2-yl)-4-(trifluoromethyl)isoxazole (**TTI-12**) was also designed (Fig. 2b). To figure out the effect of substituent on the thiophene ring of **TTI-4** and its effect on anti-cancer activity, we designed 3-(3,4-dimethoxyphenyl)-5-(5-methylthiophen-2-yl)-4-(trifluoromethyl)isoxazole (**TTI-13**) (Fig. 2b).

As $-\text{CF}_2\text{H}$ is the bioisoster of $-\text{CF}_3$, we planned to synthesize 4-(difluoromethyl)-3-(3,4-dimethoxyphenyl)-5-(thiophen-2-yl)isoxazole (**TTI-14**) and evaluate its anti-cancer activity to assess the impact of $-\text{CF}_2\text{H}$ functional group with respect to $-\text{CF}_3$. Finally, we intended to synthesize a tri-heterocyclic system introducing another biologically active core, *viz.*, pyrazolo[1,5-*a*]pyrimidine in the 3rd position of 5-(thiophen-2-yl)-4-(trifluoromethyl)-isoxazole, *i.e.*, 3-(7-phenylpyrazolo[1,5-*a*]pyrimidin-3-yl)-5-(thiophen-2-yl)-4-(trifluoromethyl)isoxazole **TTI-15** (Fig. 2b). All the designed target molecules (TMs) were planned to be synthesized following our previously developed synthetic strategy and then screened for anti-cancer activity against MCF-7, 4T1, and PC-3 cancer cell lines. By leveraging structure-activity relationship (SAR) studies, the goal is to optimize the anticancer potency and selectivity of these novel bis-heterocyclic molecules, potentially leading to the discovery of new therapeutic agents for ER α -driven cancers.

Result and discussion

1. Synthesis of designed target molecules

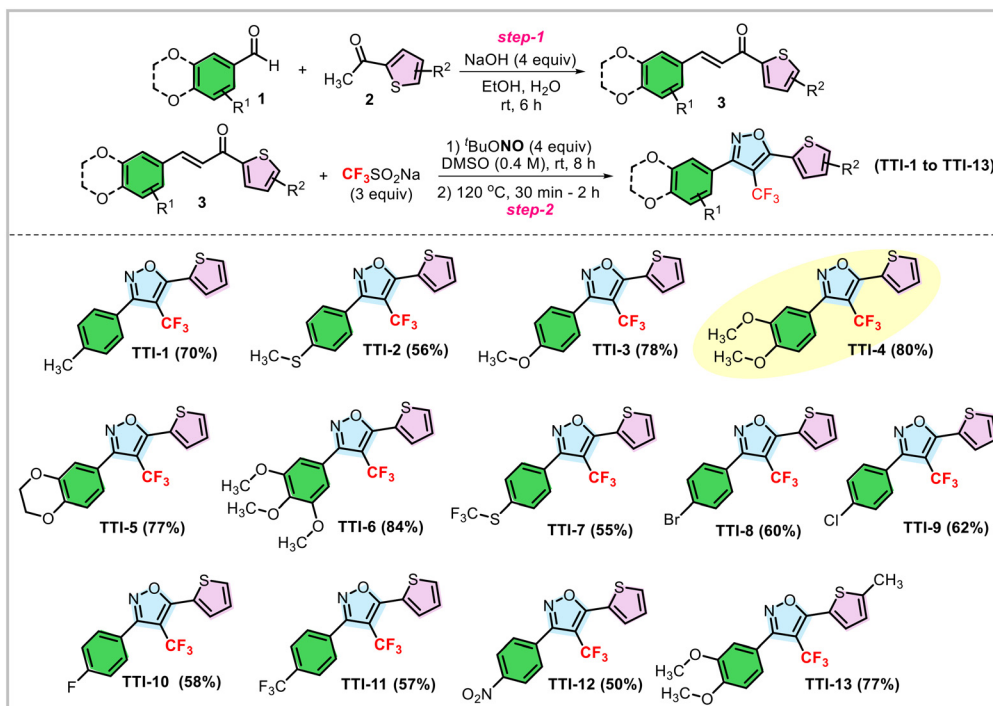
1.1. Synthesis of 3-phenyl-5-(thiophen-2-yl)-4-(trifluoromethyl)isoxazoles derivatives (TTI-1 to TTI-13). Synthesis of designed target molecules (**TTIs**) is a challenging task, and there was no direct method available for the general synthesis of this class of

molecules. Recently, we developed a metal-free, cost-effective, and sustainable synthetic strategy, *i.e.*, metal-free, cascade regio- and stereoselective trifluoromethyloximation, cyclization, and elimination strategy, with readily available α,β -unsaturated ketones for the direct synthesis of **TTIs** and derivatives by using commercially available and cheap reagents such as $\text{CF}_3\text{SO}_2\text{Na}$ and $^t\text{BuONO}$.²² In detail, the designed target molecules (**TTI-1** to **TTI-13**) were synthesized by following our previously established synthetic strategy *via* two steps, starting from commercially available feedstock materials, *i.e.*, aldehydes and acetophenones. At first, the corresponding aromatic aldehyde compound **1** was treated with the appropriate 1-(thiophen-2-yl)ethan-1-one compound **2** in the presence of NaOH to synthesize the corresponding chalcones or α,β -unsaturated ketones in moderate to good yield (50–84%). In the next step, the chalcones were converted to the target molecules (**TTI-1** to **TTI-13**) in moderate to good yield (40–70%) *via* our aforementioned synthetic strategy using $\text{CF}_3\text{SO}_2\text{Na}$ (3 equiv.) as the trifluoromethyl source, and $^t\text{BuONO}$ (4 equiv.) as an oxidant as well as the source of N and O (Scheme 1).²² The molecules were synthesized with high purity as confirmed by NMR and HPLC analysis. For example, the purity of **TTI-6** was found to be 96.6% by HPLC (Fig. S1, ESI†).

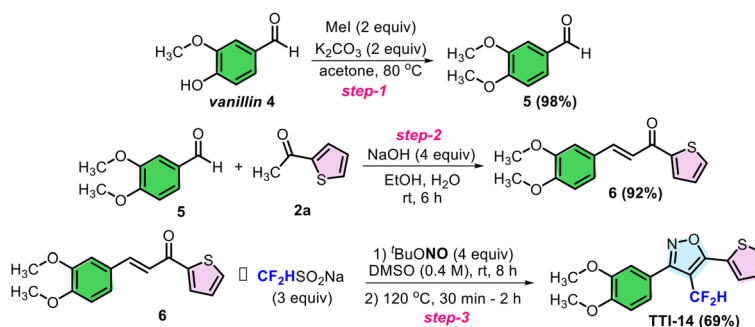
1.2. Synthesis of 4-(difluoromethyl)-3-(3,4-dimethoxyphenyl)-5-(thiophen-2-yl)isoxazole (TTI-14). The target molecule, 4-(difluoromethyl)-3-(3,4-dimethoxyphenyl)-5-(thiophen-2-yl)isoxazole (**TTI-14**) was synthesized in three steps starting from commercially available vanillin **4** which was first converted to 3,4-dimethoxybenzaldehyde **5** in 98% yield *via* a methylation reaction with methyl iodide (2 equiv.) in the presence of a base, K_2CO_3 (2 equiv.) (Scheme 2). In the next step, compound **5** was subjected to react with **2a** in the presence of NaOH (4 equiv.) in an ethanol–water mixture, which afforded the desired chalcone, *i.e.*, (*E*)-3-(3,4-dimethoxyphenyl)-1-(thiophen-2-yl)prop-2-en-1-one **6** in 92% yield. In the last step, **6** was converted to the target molecule, **TTI-14**, in 69% yield *via* the cascade regio- and stereoselective difluoromethyloximation, cyclization, and elimination reaction using $\text{CF}_2\text{HSO}_2\text{Na}$ (3 equiv.) as the difluoromethyl source, and $^t\text{BuONO}$ (4 equiv.) as an oxidant and the source of N and O.

1.3. Synthesis of 3-(7-phenylpyrazolo[1,5-*a*]pyrimidin-3-yl)-5-(thiophen-2-yl)-4-(trifluoromethyl)isoxazole. Pyrazolo[1,5-*a*]pyrimidine is an important class of fused heterocycles with significant applications in medicinal chemistry, materials science, and agrochemicals.^{23,24} Their unique structural framework imparts diverse biological activities, making them attractive scaffolds in drug discovery. Hence, we designed a five-step synthetic route starting from commercially available feedstock materials for the synthesis of 3-(7-phenylpyrazolo[1,5-*a*]pyrimidin-3-yl)-5-(thiophen-2-yl)-4-(trifluoromethyl)isoxazole (**TTI-15**), which is presented in Scheme 3. In the first step, acetophenone **7** was treated with DMF–DMA at 120 °C for the synthesis of (*E*)-3-(dimethylamino)-1-phenylprop-2-en-1-one **8** in 98% yield. In the next step, **8** was treated with 1*H*-pyrazol-5-amine **9** (1 equiv.) in the presence of AcOH to afford 7-phenylpyrazolo[1,5-*a*]pyrimidine **10** in 85% yield. Formylation of **10** by Vilsmeier–Haack reaction furnished 3-formyl-7-phenylpyrazolo[1,5-*a*]pyrimidine **11** in 90% yield. Then in the





Scheme 1 A two-step synthesis of TTI-1 to TTI-13 from commercially available feedstock materials.



Scheme 2 A three-step synthetic route to the target molecule, TTI-14, starting from vanillin.

next step, **8** was treated with 1-(thiophen-2-yl)ethan-1-one **2a** in the presence of NaOH to synthesize the corresponding α,β -unsaturated ketone, *i.e.*, (*E*)-3-(7-phenylpyrazolo[1,5-*a*]pyrimidin-3-yl)-1-(thiophen-2-yl)prop-2-en-1-one **12** in 89% yield. Finally, **12** was converted to the target molecule, **TTI-15**, in 72% yield *via* the cascade regio- and stereoselective trifluoromethyloximation, cyclization, and elimination reaction with $\text{CF}_3\text{SO}_2\text{Na}$ in the presence of $t\text{BuONO}$.

2. Evaluation of anti-cancer activities of the synthesized isoxazoles

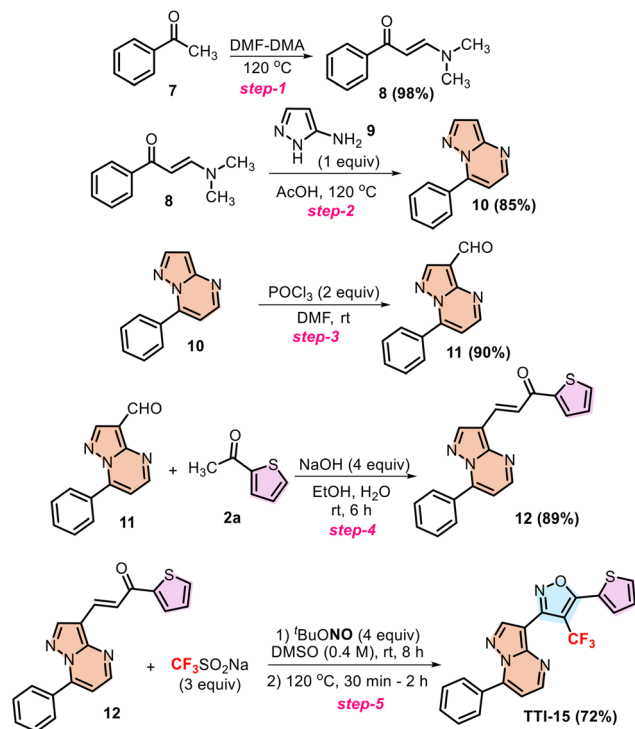
2.1. Anti-proliferative assay against cancer cell lines. In accordance with the protocol specified in section 4.2.2, all synthesized compounds were evaluated for their anticancer efficacy by the MTT assay against the human breast cancer cell

line (MCF-7), murine mammary carcinoma cell line (4T1), and the prostatic small cell carcinoma cell line (PC-3).^{25–27}

The compounds were subsequently evaluated for their IC_{50} determination at different concentrations. This research indicated that all synthesised compounds can limit the proliferation of various cancer cell types. However, **TTI-6** had the most significant antiproliferative action against MCF-7 cells among all cell lines, with an IC_{50} of 1.917 μM . According to the *in vitro* cytotoxicity assessment results from the MTT experiment, we found that the lead compound **TTI-6** is more selective against MCF-7. Consequently, we considered undertaking further research to evaluate its anti-cancer efficacy and mechanism.

2.2. Cytotoxicity towards normal HEK-293 cell line *in vitro*. We also examined the *in vitro* cytotoxicity of the synthesized molecules against a normal human embryonic kidney (HEK-293) cell line to ascertain their IC_{50} . All molecules exhibited





Scheme 3 A five-step synthetic route to the target molecule, TTI-15, starting from acetophenone.

preferential selectivity for cancer cell types while demonstrating reduced cytotoxicity toward normal cell lines. The lead compound **TTI-6** exhibited 35.62-fold selectivity for

MCF-7 cells over HEK-293 cell lines, along with 5.70 and 4-fold selectivity for other cancer cell lines (Fig. 3).

2.3. Structure–activity-relationship (SAR) analysis. After the *in vitro* evaluation of the anti-cancer activities of the newly synthesized 5-(thiophen-2-yl)-4-(trifluoromethyl)isoxazoles (**TTIs**), we became interested in analysing their structure–activity relationship (SAR). Although the trends of the anti-cancer activity of **TTIs** were found to be the same in different cancer cells, the effect was found to be more prominent against MCF-7, and hence, we decided to consider the anti-cancer activity of **TTIs** against MCF-7 for SAR analysis. It has been observed that the aryl substitution in the 3rd position of the isoxazole ring, keeping a 2-thienyl group in the 5th position and a $-\text{CF}_3$ functional group in the 4th position, had a great impact on the anti-cancer activity. The number, size, and electronic nature of the substituents in the aryl ring greatly influenced the anti-cancer activities of **TTIs**. The presence of an electron-donating or electron-withdrawing group at the *para*-position of the aryl ring significantly modulates the anti-cancer activities of **TTIs**. For example, with the increase of the electron-releasing ability of the functional groups (EDGs) such as $-\text{CH}_3$ (**TTI-1**, $\text{IC}_{50} = 24.23 \mu\text{M}$ against MCF-7), to $-\text{SCH}_3$ (**TTI-2**, $\text{IC}_{50} = 22.35 \mu\text{M}$ against MCF-7) to $-\text{OCH}_3$, (**TTI-3**, $\text{IC}_{50} = 21.5 \mu\text{M}$ against MCF-7) on the *para*-position of the aryl ring of **TTIs**, the anti-breast cancer activity increases in all cancer cell lines (entries 1–3, Table 1). Interestingly, with the increase in the number of strong electron-donating groups ($-\text{OCH}_3$), *i.e.*, **TTI-4** ($\text{IC}_{50} = 2.91 \mu\text{M}$ against MCF-7), bearing two $-\text{OCH}_3$ substituents on the *meta*- and *para*-positions of the aryl ring, exhibited 7

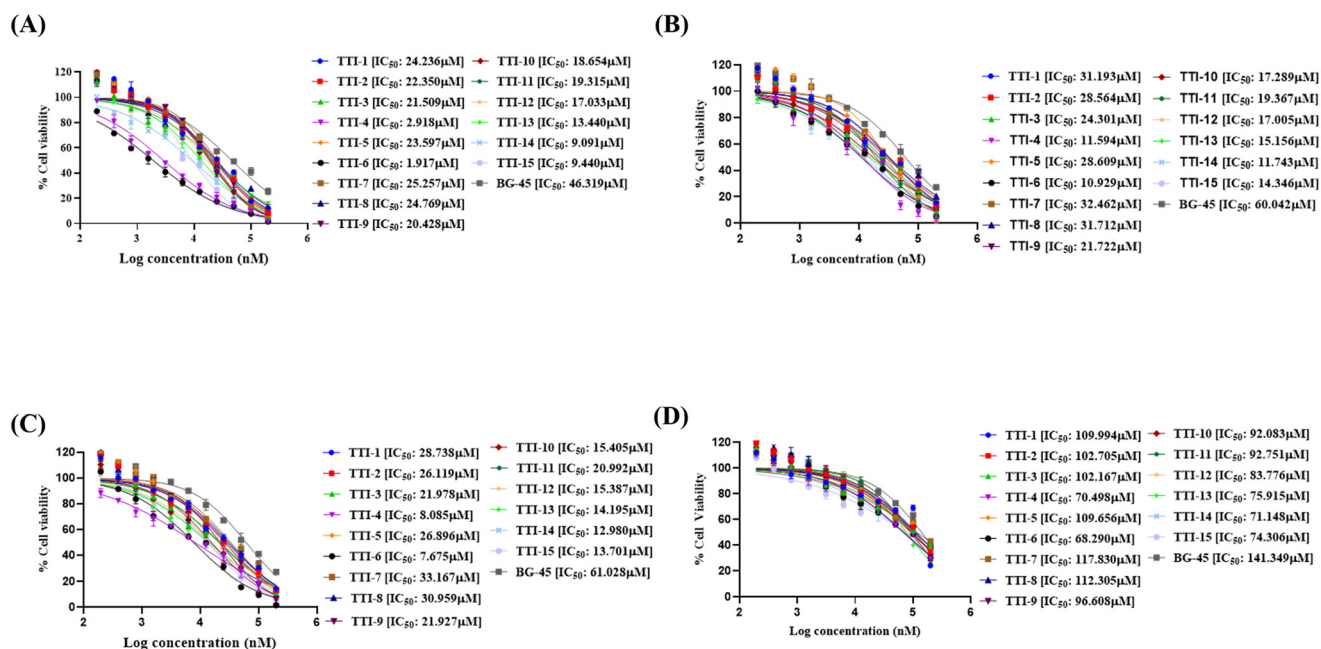


Fig. 3 IC_{50} values and dose-response curves for the TTI-1 to TTI-15 together with BG-45. Each of the compounds was evaluated at concentrations between 0.195 μM and 200 μM on (A) MCF-7, (B) 4T1, (C) PC-3, and (D) HEK-293. Cell viability was evaluated with the *in vitro* MTT test following a 48-hour treatment of cells with substances. The data is displayed as mean \pm SD ($n = 2$) and illustrated in a dose-response fashion. The IC_{50} was obtained using graph pad prism 8.0.1 and a nonlinear regression analysis method.



Table 1 Anti-proliferative assay of compounds TTI-1 to TTI-15 and BG-45 against cancer cell lines

Sl. No	Compound code	Structure of the compounds	MCF-7 IC ₅₀ (μM)	4T1 IC ₅₀ (μM)	PC-3 IC ₅₀ (μM)	HEK-293 IC ₅₀ (μM)
1	TTI-1		24.23 ± 0.15	31.19 ± 0.17	28.73 ± 0.22	109.99 ± 0.10
2	TTI-2		22.35 ± 0.07	28.56 ± 0.04	26.11 ± 0.18	102.70 ± 0.15
3	TTI-3		21.50 ± 0.11	24.30 ± 0.24	21.97 ± 0.21	102.16 ± 0.27
4	TTI-4		2.91 ± 0.13	11.59 ± 0.35	8.08 ± 0.29	70.49 ± 0.22
5	TTI-5		23.59 ± 0.17	28.60 ± 0.09	26.89 ± 0.11	109.65 ± 0.13
6	TTI-6		1.91 ± 0.09	10.92 ± 0.20	7.67 ± 0.31	68.29 ± 0.11
7	TTI-7		25.25 ± 0.18	32.46 ± 0.14	33.16 ± 0.05	117.83 ± 0.31
8	TTI-8		24.76 ± 0.14	31.71 ± 0.14	30.95 ± 0.34	112.30 ± 0.04
9	TTI-9		20.42 ± 0.21	21.72 ± 0.19	21.92 ± 0.21	96.60 ± 0.47
10	TTI-10		18.65 ± 0.15	17.28 ± 0.15	15.40 ± 0.14	92.08 ± 0.32
11	TTI-11		19.31 ± 0.24	19.36 ± 0.19	20.99 ± 0.19	92.75 ± 0.15
12	TTI-12		17.03 ± 0.12	17.00 ± 0.31	15.38 ± 0.25	83.77 ± 0.28



Table 1 (continued)

Sl. No	Compound code	Structure of the compounds	MCF-7 IC ₅₀ (μM)	4T1 IC ₅₀ (μM)	PC-3 IC ₅₀ (μM)	HEK-293 IC ₅₀ (μM)
13	TTI-13		13.44 ± 0.19	15.15 ± 0.10	14.19 ± 0.41	75.91 ± 0.16
14	TTI-14		9.09 ± 0.25	11.74 ± 0.14	12.98 ± 0.17	71.14 ± 0.21
15	TTI-15		9.44 ± 0.22	14.34 ± 0.21	13.70 ± 0.39	74.30 ± 0.25
16	BG-45		46.31 ± 0.33	60.04 ± 0.33	61.08 ± 0.17	141.34 ± 0.18

times superior anti-breast cancer activity than **TTI-3** (entry 4 vs. 3, Table 1). However, when the two $-OCH_3$ functional groups are connected covalently, *i.e.*, for 3-(2,3-dihydrobenzo[*b*][1,4]dioxin-6-yl)-5-(thiophen-2-yl)-4-(trifluoromethyl)isoxazole (**TTI-5**), the anti-cancer activity again lowered by 8 times ($IC_{50} = 23.59 \mu M$) against MCF-7 (entry 5, Table 1). We speculate that due to the loss of conformational flexibility in the fused bicyclic structure and due to the increase in rigidity, the optimal binding interactions of **TTI-5** with ER α -positive cells are hindered as compared to **TTI-4** (entry 4 vs. entry 5, Table 1). Interestingly, with the further increase in the number of $-OCH_3$ functional groups in the aryl ring, the anti-cancer activity of **TTI** increases, and **TTI-6** showed a promising anti-cancer activity with $IC_{50} = 1.91 \mu M$ (entry 3 vs. entry 4 vs. entry 6, Table 1). This result revealed that the $-OCH_3$ functional group in the aryl ring had a significant positive impact in enhancing the anti-cancer activity of **TTIs**. Moreover, when the $-SCF_3$ is introduced in the *para*-position of the aryl ring (**TTI-7**), the activity decreases significantly ($IC_{50} = 25.25 \mu M$) as compared to $-SCH_3$ bearing **TTI**, *i.e.*, **TTI-2**, ($IC_{50} = 22.35 \mu M$) (entry 7 vs. 2, Table 1). In contrast, **TTIs** bearing a halogen (Br, Cl, and F), *i.e.*, **TTI-8–TTI-10**, or electron-withdrawing groups (CF_3 and NO_2), *i.e.*, **TTI-11** and **TTI-12**, were found to have lower activity as compared to **TTI-6**. The incorporation of a methyl substituent on the thiophene ring (**TTI-13**, $IC_{50} = 13.44 \mu M$ against MCF-7) had a negative impact on the anti-cancer activity (entry 13 vs. 4, Table 1). We speculate that the addition of a methyl ($-CH_3$) group at the 5-position of thiophene (**TTI-13**) increases the steric bulk and also alters electronic properties to some extent, which may reduce binding efficiency, leading to a higher IC_{50} value ($13.44 \mu M$) as compared to **TTI-4** ($IC_{50} = 2.91 \mu M$ against MCF-7) (entry 4 vs. entry 13, Table 1). In our previous study, we showed that the presence of a $-CF_3$ group had a positive impact in

enhancing the anti-breast cancer activity of isoxazole-based molecules.²⁰ The $-CF_2H$ group serves as a bioisostere of $-CF_3$, differing by the replacement of one fluorine atom with hydrogen, and thus, it is an important functional group in medicinal chemistry. However, this small structural change leads to a notable reduction in potency in **TTI** as **TTI-4** with a $-CF_3$ group ($IC_{50} = 2.91 \mu M$ against MCF-7) is found to have much better activity than that of **TTI-14** with $-CF_2H$ group ($IC_{50} = 9.01 \mu M$ against MCF-7), which eventually revealed that the $-CF_3$ group provides superior interactions with the target binding site than that of $-CF_2H$ (entry 4 vs. entry 14, Table 1). The higher electronegativity and stronger hydrophobicity of $-CF_3$ likely enhance receptor binding, whereas $-CF_2H$ introduces a hydrogen-bond donor, which may alter the molecular conformation or disrupt optimal hydrophobic interactions. The tri-heteroaryl core, *i.e.*, 3-(7-phenylpyrazolo[1,5-*a*]pyrimidin-3-yl)-5-(thiophen-2-yl)-4-(trifluoromethyl)isoxazole (**TTI-15**, $IC_{50} = 9.44 \mu M$ against MCF-7) was found to be less active than that of **TTI-4** and **TTI-6**.

2.4. Apoptosis assay²⁶. Numerous studies have demonstrated that cytotoxic effects induce cell death through apoptotic pathways. A flow cytometry study utilizing the annexin-V/FITC-PI apoptotic test was conducted to elucidate the apoptosis process in MCF-7 cells, assessing the impact of $1.917 \mu M$ (IC_{50}) of **TTI-6** on cell cycle state during a 48-hour period. The chosen doses have already demonstrated a significant effect on MCF-7 cells, and the concentrations were established based on the MTT assay data. The results indicated that the treatment of **TTI-6** significantly enhanced apoptotic activity in cells. In comparison to the control at $2.1 \pm 0.9\%$ and the standard compound **BG-45** at $15.6 \pm 1.7\%$, compound **TTI-6** exhibited a total apoptotic percentage of $50.0 \pm 1.3\%$ (Q2 and Q4). These results indicate that the programmed cell death mechanism induced by lead



compound **TTI-6** significantly promotes apoptosis in cancer cells.

2.5. Cell cycle analysis²⁵. Alongside the apoptotic assay findings, the cell cycle progression of MCF-7 cells was examined with compound **TTI-6**, and the distribution of the cell population throughout several cell cycle stages was evaluated using flow cytometry. In the cell cycle experiment, MCF-7 cells were subjected to a 48-hour treatment with compound **TTI-6** at a concentration of 1.917 μM (IC_{50}). In comparison to the control and the standard compound **BG-45**, the results indicate that compound **TTI-6** is highly effective in inhibiting DNA synthesis during the S-phase, exhibiting a population of 1.5%, while simultaneously promoting G2/M-phase progression with a population of 34.8% relative to both the control and **BG-45**. The G0/G1-phase distribution exhibits minor variations, with cells treated with **TTI-6** displaying a little elevated percentage (63.7%) in this phase relative to the standard compound (58.4%) and the control (62.1%). The data indicate that the lead compound **TTI-6** uniquely influences cell cycle regulation in comparison to control and standard compound-treated cells.

2.6. Nuclear staining²⁶. A nuclear staining assay was conducted utilizing DAPI and AO as staining dyes to assess the phenomenon of apoptosis in cancer cells using a laser scanning confocal microscope (LSCM). Treatment of MCF-7 cells with compound **TTI-6** at IC_{50} for 48 hours induced a significant alteration in cell morphology compared to control and **BG-45**-treated cells, as depicted in Fig. 4. These findings illustrate nuclear disintegration in treated cells and suggest an apoptotic cell death mechanism. The fluorescence pattern

in AO staining transitioned from green (indicating normal cellular DNA) to orange (indicating nicked cellular DNA). The elevated fluorescence of AO in cells treated with compound **TTI-6** indicated a significantly greater degree of chromosomal condensation compared to untreated cells, suggesting that the molecule is cytotoxic. The cells exposed to compound **TTI-6** exhibited more apoptosis compared to the control and normal **BG-45** treated cells (Fig. 5 and 6).

2.7. Assessment of ROS production²⁶. A multitude of cancer cells demonstrate elevated basal levels of reactive oxygen species (ROS) in comparison to normal cells. This may arise from the heightened metabolic requirements of rapidly proliferating cancer cells and mitochondrial impairment. Increased amounts of reactive oxygen species (ROS) can harm DNA, leading to genomic instability and the emergence of genetic abnormalities that promote cancer growth. Chemotherapy agents can produce reactive oxygen species (ROS) as a consequence of their action, resulting in DNA damage and apoptosis in neoplastic cells. Consequently, we examined whether the compound **TTI-6** may induce ROS generation in cancer cells. Compound **TTI-6**-treated cells exhibited a significant increase in relative fluorescence intensity at the IC_{50} dose compared to the control (1% DMSO-treated cells). Preliminary *in vitro* tests indicate that the lead compound **TTI-6** generated reactive oxygen species, leading to oxidative stress, which caused cell cycle phase arrest and initiated apoptosis *via* many intrinsic mechanisms (Fig. 7).

3. *In silico* analysis of **TTI-4** and **TTI-6**

3.1. Validation of docking protocol and ligand-receptor binding analysis by molecular docking and MMGBSA ΔG .

Following target selection, energy minimization, and grid development in the catalytic binding pocket of ER α (PDB ID: 3ERT), the receptor was validated for ligand-receptor docking. The co-crystal ligand 4HT was prepared using LigPrep at pH 7.4, and XP docking was performed to assess the binding pose. The RMSD after superimposition of the co-crystal ligand on the minimized protein was 0.7939 Å, which is below the 2 Å threshold, confirming the validation of the docking protocol (Fig. 8).²⁸

Compounds **TTI-6**, **TTI-14**, **TTI-3**, **TTI-5**, and **TTI-4** were energy minimized using the LigPrep module with the Epik tool, including desalting, chirality determination, and tautomer generation. The minimized compounds were docked using extra precision (XP) and standard precision (SP) docking modes for the evaluation of binding affinity to ER α . The MM/GBSA ΔG free binding energy was calculated using the VSGB2.0 solvation model, with results presented in Table 2 (Fig. 9).

The docking scores for **TTI-6**, **TTI-14**, **TTI-3**, and **TTI-5** ranged from $-8.391 \pm 1.378 \text{ kcal mol}^{-1}$ to $-5.638 \pm 0.946 \text{ kcal mol}^{-1}$, while **TTI-4** scored $-7.471 \pm 0.564 \text{ kcal mol}^{-1}$. Among them, **TTI-6** represented the best docking score of $-8.391 \text{ kcal mol}^{-1}$ and the lowest MM/GBSA ΔG of $-34.45 \text{ kcal mol}^{-1}$. The binding interactions revealed hydrophobic contacts with leucine residues (LEU346, LEU384, and LEU387), polar

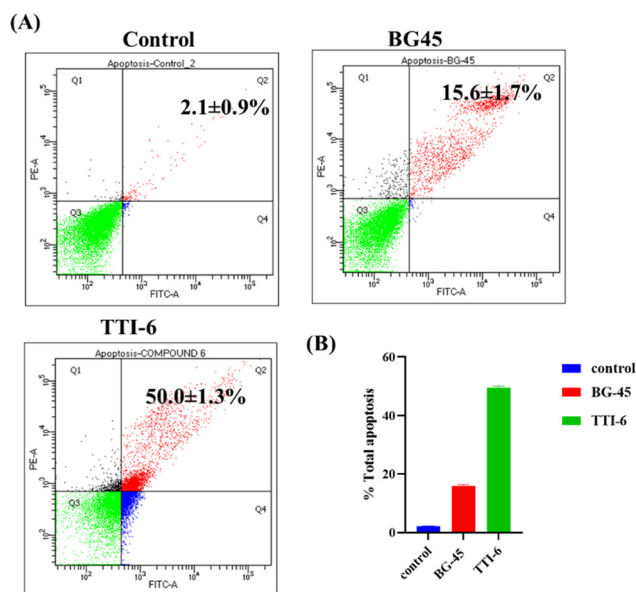


Fig. 4 (A) Flow cytometric study of apoptosis utilizing the annexin V/PI assay double staining. The same cultures of MCF-7 cells were treated with vehicle control, **BG-45**, and **TTI-6** for 48 hours (Q1 – necrotic cells, Q2 – late apoptosis, Q3 – live cells, Q4 – early apoptotic cells) at their respective *in vitro* IC_{50} values (the X and Y axes show the intensities of annexin V and propidium iodide). (B) Graphical representation of overall apoptotic percentage analysis in MCF-7 cells.



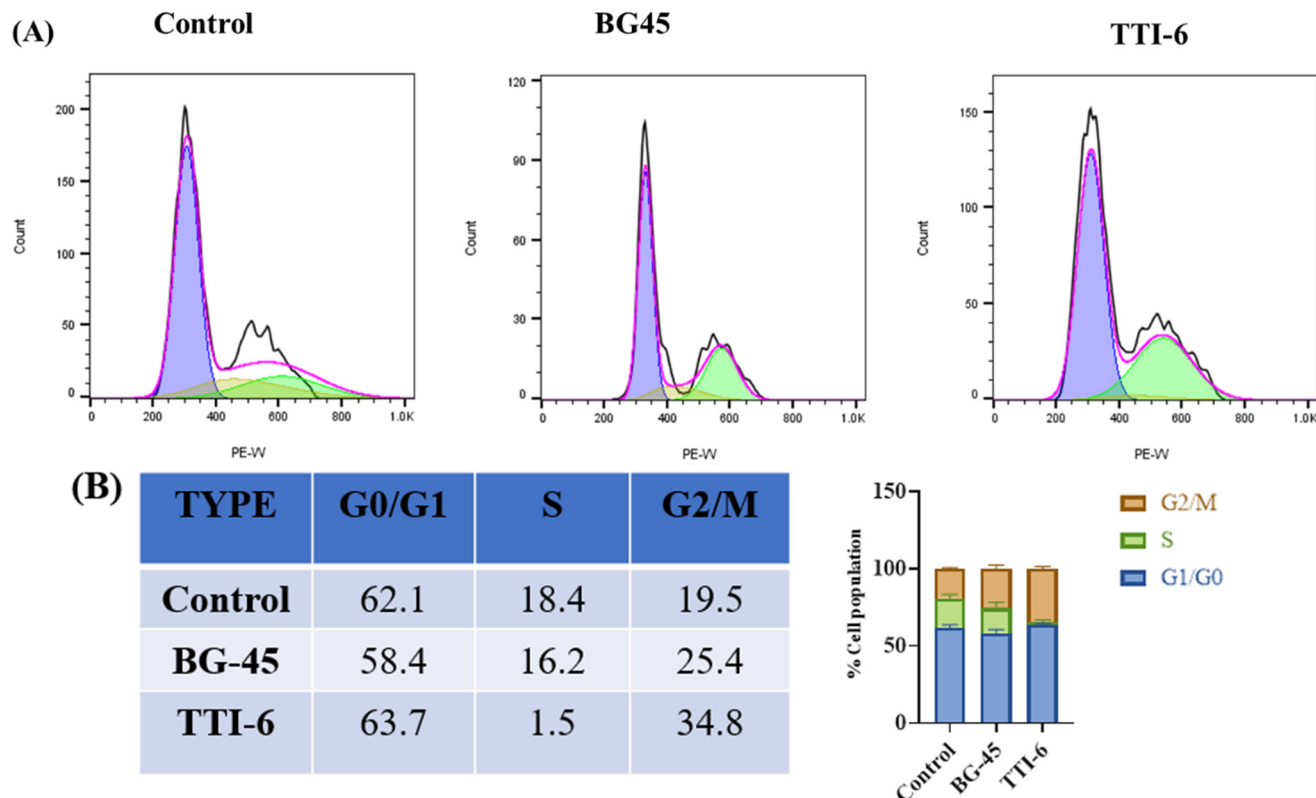


Fig. 5 (A) Cell cycle analysis in MCF-7 cells treated for 48 hours with vehicle, reference drug BG-45, and compound TTI-6 at IC_{50} concentrations. Cell cycle analysis was performed after the appropriate treatment durations and was then evaluated using a flow cytometer (BD Aria III) (B). G1, S, and G2/M phases of the cell cycle in MCF-7 cells are represented graphically and in tabular form, respectively.

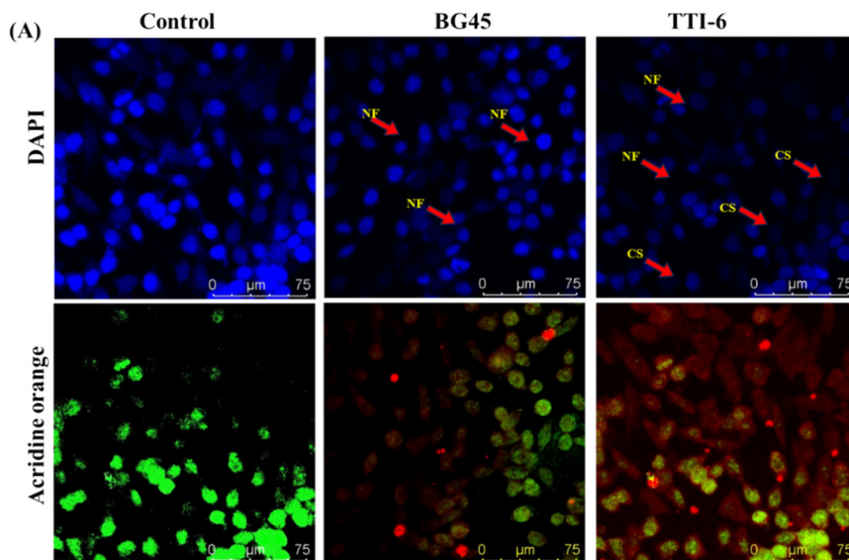


Fig. 6 Nuclear morphology analysis by nuclear staining experiment *in vitro* in MCF-7 cells after treatment with IC_{50} concentrations of BG-45 and compound TTI-6 along with control (A) MCF-7 cells using the staining solutions of DAPI and AO after the treatment period. NF symbolizes nuclear fragmentation, while CS represents cell shrinkage. The stained nuclei were observed using a laser scanning confocal microscope DMI8 (Leica microsystems, Germany) at 63 \times magnification.

interaction with THR347, positive charge with ARG394, and negative charges with GLU353 and ASP351. Therefore, it was observed that the compound **TTI-6** could be an ER α inhibitor

with the aromatic hydrophobic interaction by disruption of helix 12, the primary hallmark for ER α inhibition for anti-breast cancer therapeutics. The compounds **TTI-6**, **TTI-14**,



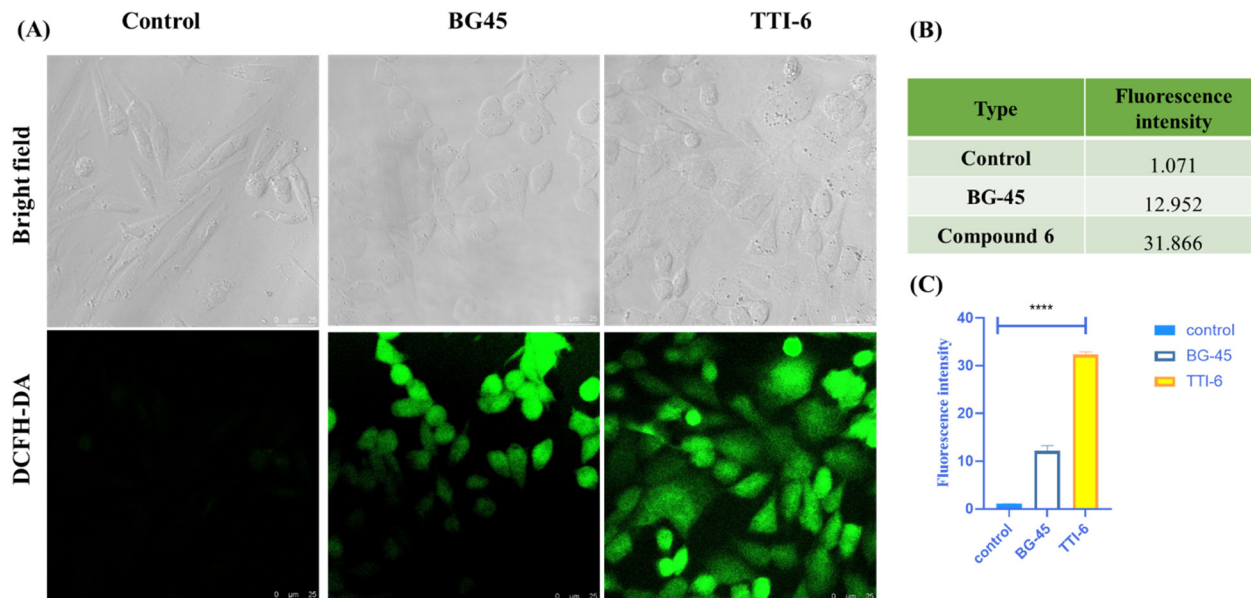


Fig. 7 Intracellular ROS generation by DCFH-DA in MCF-7 cells after 48 hours of treatment with IC_{50} doses of BG-45 and compound TTI-6, as well as a control. (A) MCF-7 cells stained with DCFH-DA dye after treatment time, (B) table reflecting the fluorescence intensity values quantified by the ImageJ program, and (C) plot of fluorescence intensity obtained. The ROS generation was visualized using a Leica microscope at 60 \times magnification and a laser scanning confocal microscope DMI8 (Leica microsystems, Germany). Scale bars are 25 μm long. The acquired results are the mean standard deviation ($n = 2$); **** p 0.0001. ImageJ software was used to calculate the fluorescence intensity. The significance was determined using one-way ANOVA, and the graph was created in GraphPad Prism 8.0.1.

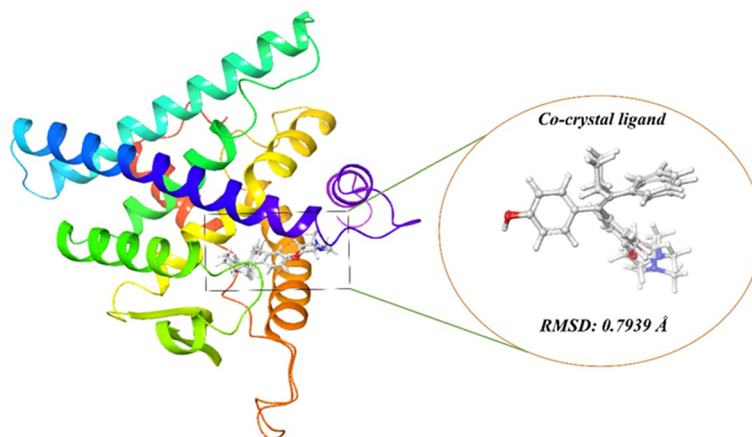


Fig. 8 Validation of the docking protocol by the superimposition of the docked co-crystal ligand with the minimized HER α co-crystal ligand and the RMSD was observed at 0.7939 Å.

TTI-3, and TTI-5 showed similar interactions to TTI-4 at the antagonist binding site, as shown in Fig. S2[†] (Table 3).

3.2. Induced fit docking (IFD) analysis. The induced fit docking protocol was used to revalidate the molecular docking and MMGBSA analysis, as there is a chance of false positive results, and the receptor is not flexible in the docking studies for the generation of multiple conformations. IFD protocol utilizes both Glide and Prime to produce more realistic outcomes after initial docking, refinement, and further re-docking. IFD treats the protein and ligand in a more flexible way than only grid-based

docking to understand the binding results. The more the poses generate, the better the stability and affinity towards the target. In the present study, TTI-6 was selected as the lead molecule due to its excellent binding affinity towards HER α and anticancer activity towards MCF-7, the human breast cancer cell line. It produced 22 poses after IFD analysis extended sampling, while TTI-4 produced only eight poses for binding with HER α . TTI-6 showed similar interactions to XP docking, although in pose (C), it showed a water bridge H-bond interaction with TRP383. The IFD scores for TTI-6 for all three poses are (A) -10 523.21, (B) -10 520.72, and (C) -10



Table 2 Structure, docking score, and MMGBSA ΔG of compounds – TTI-6, TTI-14, TTI-3, TTI-5, and TTI-4

Compounds	Structure	Docking score (mean \pm SD), $n = 2$, kcal mol ⁻¹	MMGBSA ΔG kcal mol ⁻¹
TTI-6		-8.391 ± 1.378	-34.45
TTI-14		-7.306 ± 0.403	-23.80
TTI-3		-6.965 ± 0.090	-29.80
TTI-5		-5.638 ± 0.946	-34.17
TTI-4		-7.471 ± 0.564	-29.58

514.69 [Fig. 10A–C]. In the top two poses, positive charge interaction was observed with ARG394G, as reported in Fig. S3, ESI†. TTI-6 showed a better IFD score than TTI-4 with an IFD score of (A) $-10\,510.36$, (B) $-10\,510.26$, and (C) $-10\,476.48$ in the top three poses [Fig. 11D–F and S4, ESI†]. Therefore, it was observed that TTI-6 showed significant binding affinity, docking score, as well as IFD score towards HER α for anticancer activities when compared with TTI-4.

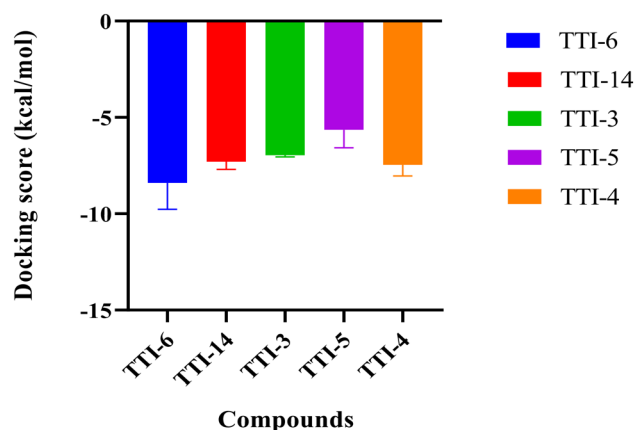


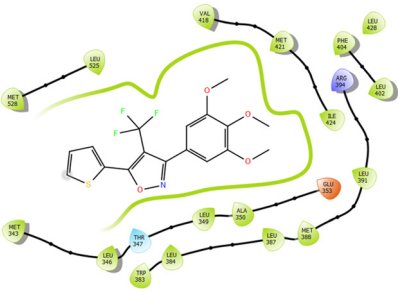
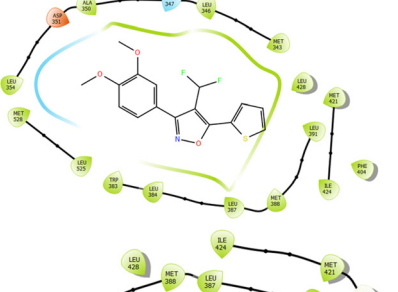
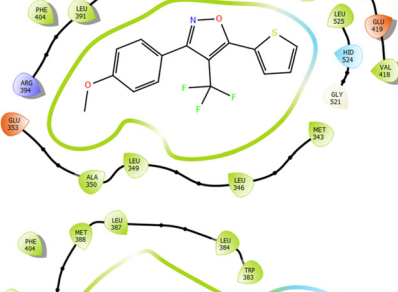
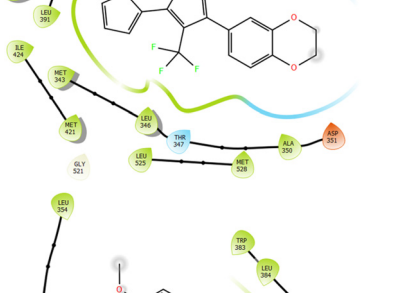

Fig. 9 Graphical representation of docking score analysis of compounds – TTI-6, TTI-14, TTI-3, TTI-5, and TTI-4, with $n = 2$ (the data was represented with mean \pm SD) [calculation was provided in Table S2, ESI†].

3.3. MD simulation. The molecular docking protocols, such as Glide-based docking and induced fit docking, cannot mimic the pharmacological condition and cannot predict the protein conformational changes during the ligand binding at the catalytic binding site. Therefore, ligand–receptor molecular dynamics simulation was employed with the lead TTI-6 and TTI-4, which provided molecular insight into the antagonistic binding pocket and changes in protein folding. The study was performed using the *Desmond* application at 300 K temperature, 1.013 bar pressure on an SPC model using an OPLS4 force field.

For TTI-6–HER α complex, the mean RMSD after 100 ns dynamics simulation ligand with respect to protein and with respect to ligand were 5.963 ± 0.701 Å and 1.317 ± 0.169 Å respectively, protein C α and backbone were 3.044 ± 0.419 Å, and 3.054 ± 0.419 Å respectively, protein side chain and heavy chain were 4.191 ± 0.464 Å, and 3.564 ± 0.443 Å respectively. The average RMSF of HER α was 1.266 ± 0.863 Å throughout the simulation, and the ligand properties include mean radius of gyration (rGyr) of 4.031 ± 0.035 Å, mean solvent accessibility surface area (SASA) of 40.478 ± 14.243 Å², and mean polar surface area (PSA) of 65.862 ± 4.705 Å². Binding interaction with LYS529 was also observed by π –cation interaction and positively charged interaction, and various hydrophobic interactions with LEU384, LEU391, LEU387, ALA350, LEU539, MET388, ILE424, MET421, LEU525, and LEU346 at the catalytic binding pocket, as reported in Fig. 12.



Table 3 2D interaction diagram of compounds – TTI-6, TTI-14, TTI-3, TTI-5, and TTI-4, along with their important interactions

Compounds	2D interaction	Important interactions
TTI-6		Hydrophobic: TRP383, LEU384, LEU387, MET388, LEU391, LEU402, PHE404, MET343, LEU346, LEU349, ALA350, ILE424, MET421, VAL418, LEU525, MET528, polar: THR347, +ve charge: ARG394, -ve charge: GLU353
TTI-14		Hydrophobic: TRP383, LEU384, LEU387, MET388, LEU391, PHE404, MET343, LEU346, ALA350, LEU354, ILE424, MET421, LEU428, LEU525, MET528, polar: THR347, -ve charge: ASP351
TTI-3		Hydrophobic: LEU384, LEU387, MET388, LEU391, LEU428, PHE404, MET343, LEU346, LEU349, ALA350, VAL418, MET421, ILE424, LEU525, polar: HID524, +ve charge: ARG394, -ve charge: GLU419, GLU353, glycine: GLY420, GLY521
TTI-5		Hydrophobic: TRP383, LEU384, LEU387, MET388, LEU391, PHE404, ILE424, MET421, LEU428, PHE404, MET343, LEU346, ALA350, LEU525, MET528, polar: THR347, -ve charge: GLU351, glycine: GLY521
TTI-4		Hydrophobic: TRP383, LEU384, LEU387, MET388, LEU391, ILE424, MET421, LEU428, MET343, LEU346, ALA350, LEU354, LEU525, MET528, polar: THR347, -ve charge: ASP351



Note: LEU: leucine, MET: methionine, THR: threonine, ASP: aspartic acid, TRP: tryptophan, GLU: glutamic acid, GLY: glycine, ARG: arginine, VAL: valine, PHE: phenylalanine, HID: histidine, ILE: isoleucine.



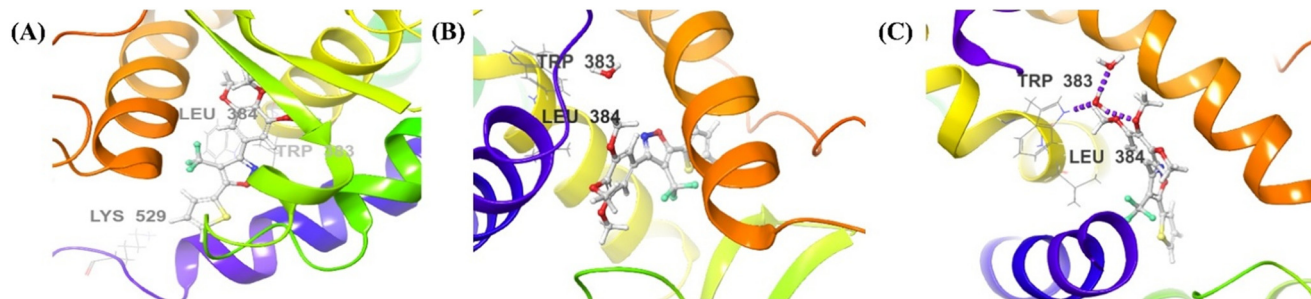


Fig. 10 3D interaction diagram for induced fit docking of TTI-6 and HER α in top three poses – (A) –10 523.21, (B) –10 520.72, and (C) –10 514.69.

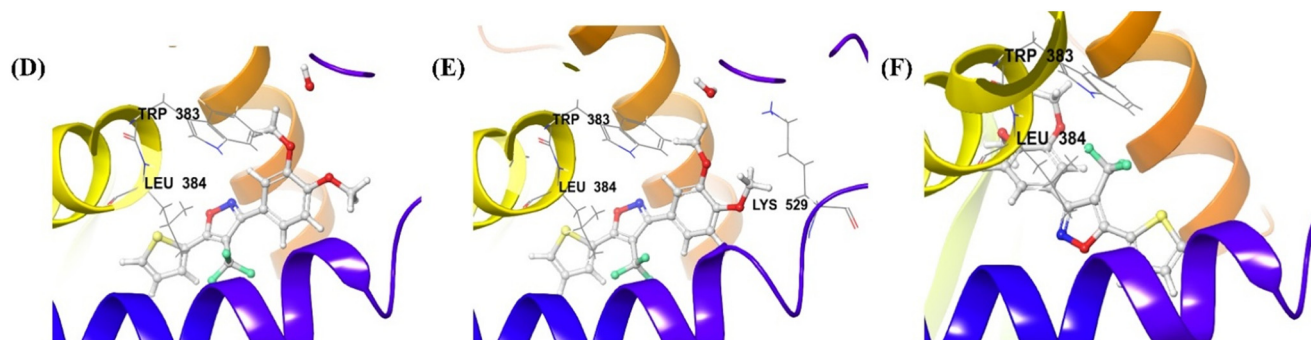


Fig. 11 3D interaction diagram for induced fit docking of TTI-4 and HER α in top three poses (D) –10 510.36, (E) –10 510.26, and (F) –10 476.48.

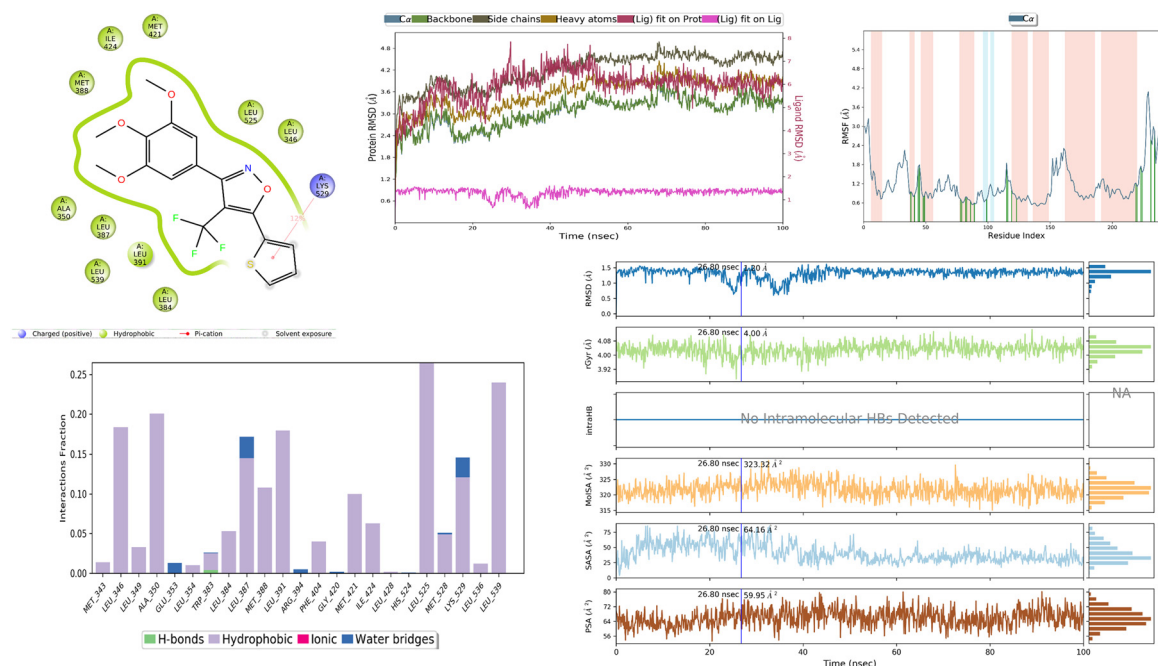


Fig. 12 The RMSD, RMSF, and binding interactions of TTI-6-HER α complex, along with the ligand properties, such as rGyr, MolSA, SASA, and PSA.

For TTI-4-HER α complex, the mean RMSD after 100 ns dynamics simulation ligand with respect to protein and with respect to ligand were 6.008 ± 0.799 Å and 1.725 ± 0.367 Å respectively, protein C α and backbone were 2.811 ± 0.383 Å, and 2.853 ± 0.408 Å respectively, protein side chain and heavy

chain were 4.048 ± 0.386 Å, and 3.406 ± 0.382 Å respectively. The average RMSF of HER α was 1.342 ± 0.954 Å throughout the simulation, and the ligand properties include the mean radius of gyration (rGyr) of 3.938 ± 0.047 Å, mean solvent accessibility surface area (SASA) of 14.563 ± 6.82 Å², and mean polar surface



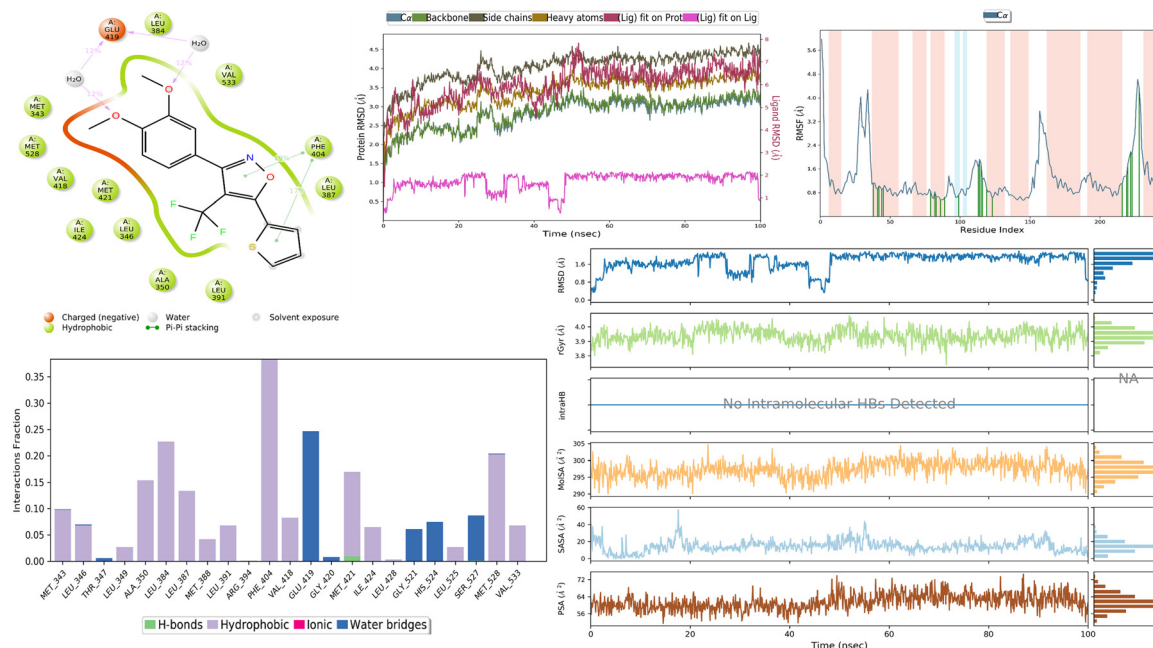


Fig. 13 The RMSD, RMSF, and binding interactions of the **TTI-4**–HER α complex, along with the ligand properties, such as rGyr, MolSA, SASA, and PSA.

area (PSA) of $61.513 \pm 3.791 \text{ \AA}^2$. Binding interaction with PHE404 was also observed by π – π stacking interaction, GLU419 with water bridge H-bond and negatively charged interaction, and various hydrophobic interactions with LEU384, MET343, MET520, VAL418, MET421, LEU346, ILE424, ALA350, LEU391, LEU387, PHE404, and VAL533 at the catalytic binding pocket, as reported in Fig. 13. The comparison of RMSD and RMSF was reported in Table 4.

RMSD measures the mean deviation in the position of atoms of the ligand or the protein over time during a simulation. Low RMSD indicates that the ligand remains stable in the catalytic binding site, implying a strong and consistent interaction. Ligand RMSD is relative to the protein binding site and provides insights into how well the ligand is anchored and the stability of the ligand–receptor complex. The complex of **TTI-6**–HER α showed less RMSD with respect to protein, as well as ligand, than the complex of **TTI-4**–HER α [Table 4]; therefore, the binding affinity and stability are better for **TTI-6** than **TTI-4** in HER α . RMSF indicates the flexibility of individual residues of the protein over time during a simulation. In the region where no α -helix or β -sheet was observed, the fluctuation was more, and the fluctuation was more in the **TTI-4**–HER α complex than in the **TTI-6**–HER α complex, as reported in Table 4. The lower RMSF value suggests a stable interaction between the protein HER α and **TTI-6** than HER α and **TTI-4**. Furthermore, analyzing the

ligand properties – like rGyr, MolSA, SASA, and PSA – it was observed that the two compounds represented similar results. However, the **TTI-6**–HER α showed more stability, flexibility, and compactness throughout the simulation than the **TTI-4**–HER α complex. Further, ADMET analysis will provide insight into whether **TTI-6** can be druggable and its pharmacokinetic and toxicity profiling.

3.4. Drug-likeness and ADMET studies. The drug-likeness and ADME analysis were performed using the QikProp tool of Maestro, and further, the toxicity analysis was performed with the open server pkCSM. Neither compound violated the Lipinski rule of five and represented drug-like properties throughout the analysis and 100% human oral absorption, as reported in Table 5. Further, other descriptors were analyzed, such as water solubility (QPlogS), Caco2 cell permeability in nm s^{-1} (QPpCaco), predicted blood–brain partition coefficient (QPlogBB), predicted MDCK cell permeability in nm s^{-1} (QPMDCK), and human serum albumin binding prediction (QPlogKhsa), which was reported in Table 6.

Both the compounds, **TTI-6** and **TTI-4**, represented excellent results in the ADME analysis, and both of them showed similar results for drug-likeness properties. Further, the toxicity analysis is represented in Fig. 1. It was observed that **TTI-6** showed lesser toxicity in various toxicity descriptors – minnow toxicity, *T. pyriformis* toxicity, max tolerated dose (human), and oral rat

Table 4 Comparison table for RMSD and RMSF of complexes – **TTI-6** and **TTI-4** with HER α

Compounds	RMSD Å (mean \pm SD), $n = 1000$ (w.r.t protein HER α)	RMSD Å (mean \pm SD), $n = 1000$ (w.r.t ligand)	Protein RMSF (mean \pm SD), $n = 246$
TTI-6	5.963 ± 0.701	1.317 ± 0.169	1.266 ± 0.863
TTI-4	6.008 ± 0.799	1.725 ± 0.367	1.342 ± 0.954



Table 5 Analysis of druglikeness and rule of five

Compounds	Molecular weight	Hydrogen bond donor	Hydrogen bond acceptor	QPlogP(o/w)	Percent human oral absorption	Rule of five violations
TTI-6	385.357	0	3.750	4.603	100	0
TTI-4	355.331	0	3.000	4.616	100	0

Table 6 Other ADME properties

Compounds	QPlogS	QPPCaco	QPlogBB	QPPMDCK	QPlogKhsa
TTI-6	-5.425	4095.315	0.296	10 000	0.490
TTI-4	-5.465	3888.857	0.352	10 000	0.557
Acceptable range	-6.5–0.5	Excellent >500	-3.0–1.2	Excellent >500	-1.5–1.5

chronic toxicity, although slightly higher in oral rat acute toxicity descriptor than compound **TTI-4** [detailed table was provided in Table S3, ESI† (Fig. 14)].

3.5. In silico SAR analysis of the lead molecule (TTI-6). The *in silico* studies revealed the importance of various functional groups or moieties of the lead molecule in bringing the crucial interactions with HER α (PDB ID: 3ERT) and thus enhancing the anti-breast cancer activity. While the thiophene moiety on the 5th position of isoxazole interacts with LYS 529 of the protein, the -CF₃ group on the 4th position was found to be crucial in enhancing the anti-cancer activity. Notably, the H-bond acceptor ability of the three -OCH₃ groups in the benzene ring at the 3rd position helped in bringing a strong interaction with the TRP383 through H-bonding with water molecules, as reported in Fig. 15.

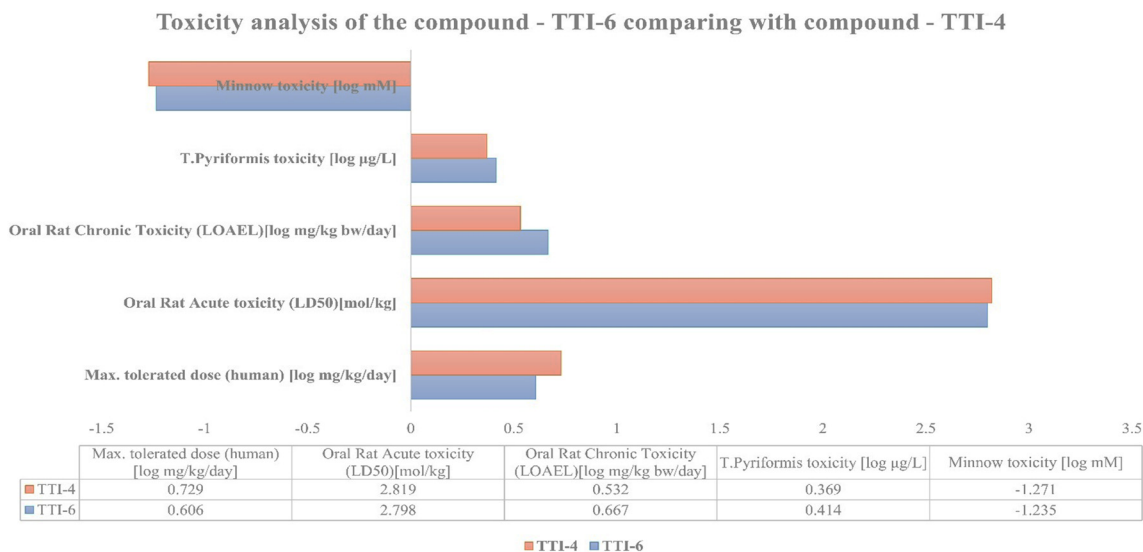
4. Materials and methods

4.1. General information for chemistry

All the required chemicals were purchased from various companies and used without purification. The products

were characterized by ¹H and ¹³C NMR. NMR spectra were recorded on a Bruker 400 MHz instrument (400 MHz for ¹H NMR and 100 MHz for ¹³C NMR). Copies of ¹H and ¹³C NMR spectra can be found at the end of the ESI†. ¹H NMR data are reported in units, parts per million (ppm), and were measured relative to residual chloroform (7.26 ppm) in the deuterated solvent. ¹³C NMR data are reported in ppm relative to deuteriochloroform (77.00 ppm), and all were obtained with ¹H decoupling. Coupling constants were reported in Hz. Reactions were monitored by thin layer chromatography (TLC) and ¹H-NMR of the crude reaction mixture using 1,3,5-trimethoxybenzene as the internal standard. Mass spectral data of unknown compounds were obtained on a high-resolution mass spectrometer, HRMS. Melting points of unknown compounds were recorded on a KRUSSE Optronic M3000 apparatus.

4.1.1. Synthesis of 3-phenyl-5-(thiophen-2-yl)-4-(trifluoromethyl)isoxazoles derivatives. 3-Phenyl-5-(thiophen-2-yl)-4-(trifluoromethyl)isoxazoles derivatives were successfully synthesized *via* a two-step reaction, starting from the feedstock

**Fig. 14** Toxicity analysis and comparison of TTI-6 and TTI-4.

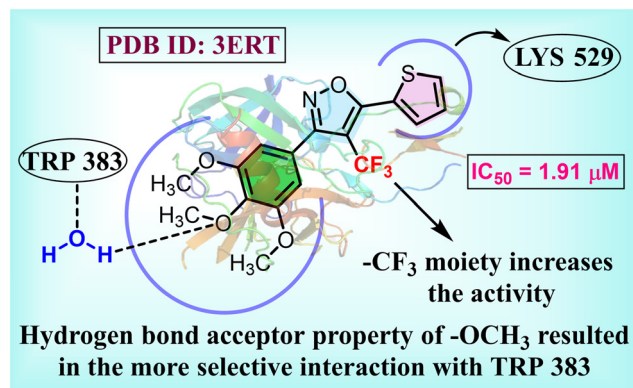


Fig. 15 *In silico* SAR analysis of TTI-6.

materials, *i.e.*, substituted benzaldehydes (**1**) and substituted 1-(thiophen-2-yl)ethan-1-one (**2**) (Scheme 1).

Step-1: To a solution of the appropriate 1-(thiophen-2-yl)ethan-1-one compound **2** (10 mmol, 1 equiv.) in ethanol-water mixture (4:1) (20 mL), added an aqueous solution of NaOH (4 equiv.) followed by appropriate benzaldehyde **1** (10 mmol, 1 equiv.). The mixture was stirred at low temperature for five hours, and the progress of the reaction was monitored by TLC. Then, the resulting solution was extracted with ethyl acetate thrice (3 × 10 mL), and the combined organic layer was washed with water (3 × 10 mL). The organic layer was dried with anhydrous Na₂SO₄, and the solvent was evaporated under reduced pressure to afford the crude product which was purified by column chromatography to afford **3** in a quantitative yield.

Step-2: Freshly synthesized **3** (0.5 mmol, 1 equiv.) and CF₃-SO₂Na (3 equiv.) were taken in an oven-dried 10 mL sealed tube, and DMSO (1.25 mL, 0.4 M) was added to that mixture. Then TBN (4 equiv.) was added to the reaction mixture, and it was stirred at room temperature. The progress of the reaction was monitored by TLC, then the sealed tube was closed very tightly and sealed properly, and the reaction mixture was heated at 120 °C in an oil bath for 30 min. Then the resulting solution was extracted with ethyl acetate thrice (3 × 10 mL), and the combined organic layer was washed with water (3 × 10 mL). The organic layer was dried with anhydrous Na₂SO₄, and the solvent was evaporated under reduced pressure to afford the crude product, which was purified by column chromatography to afford 3-phenyl-5-(thiophen-2-yl)-4-(trifluoromethyl)isoxazoles derivatives (**TTI-1** to **TTI-13**) in good to moderate yield.

4.1.2. Synthesis of 4-(difluoromethyl)-3-(3,4-dimethoxyphenyl)-5-(thiophen-2-yl)isoxazole. 4-(Difluoromethyl)-3-(3,4-dimethoxyphenyl)-5-(thiophen-2-yl)isoxazole derivatives were successfully synthesized *via* a three-step reaction, starting from the feedstock materials, *i.e.*, vanillin (**4**) and substituted 1-(thiophen-2-yl)ethan-1-one (**2**) (Scheme 2).

Step-1: Vanillin (10 mmol, 1 equiv.) and K₂CO₃ (20 mmol, 2 equiv.) were taken in an oven-dried round-bottom flask, and acetone (10 mL) was added to the mixture, followed by methyl iodide (20 mmol, 2 equiv.). Then the reaction mixture

was stirred at 80 °C for 8 h. The progress of the reaction was monitored by TLC. Then, the resulting solution was extracted with ethyl acetate thrice (3 × 10 mL), and the combined organic layer was washed with water (3 × 10 mL). The organic layer was dried with anhydrous Na₂SO₄, and the solvent was evaporated under reduced pressure to afford the crude product 3,4-dimethoxybenzaldehyde (**5**). After that, the crude product was used for the next step without any further purification.

Step-2: To a solution of 1-(thiophen-2-yl)ethan-1-one **2a** (10 mmol, 1 equiv.) in ethanol-water mixture (4:1) (20 mL), add an aqueous solution of NaOH (4 equiv.) followed by 3,4-dimethoxybenzaldehyde **5** (10 mmol, 1 equiv.). The mixture was stirred at a low temperature for five hours, and the progress of the reaction was monitored by TLC. Then, the resulting solution was extracted with ethyl acetate thrice (3 × 10 mL), and the combined organic layer was washed with water (3 × 10 mL). The organic layer was dried with anhydrous Na₂SO₄, and the solvent was evaporated under reduced pressure to afford the crude product, which was purified by column chromatography to afford **6** in a quantitative yield.

Step-3: Freshly synthesized **6** (0.5 mmol, 1 equiv.) and CF₃-HSO₂Na (3 equiv.) were taken in an oven-dried 10 mL sealed tube, and DMSO (1.25 mL, 0.4 M) was added to that mixture. Then TBN (4 equiv.) was added to the reaction mixture, and it was stirred at room temperature. The progress of the reaction was monitored by TLC, then the sealed tube was closed very tightly and sealed properly, and the reaction mixture was heated at 120 °C in an oil bath for 30 min. Then the resulting solution was extracted with ethyl acetate thrice (3 × 10 mL), and the combined organic layer was washed with water (3 × 10 mL). The organic layer was dried with anhydrous Na₂SO₄, and the solvent was evaporated under reduced pressure to afford the crude product, which was purified by column chromatography to afford 3-phenyl-5-(thiophen-2-yl)-4-(trifluoromethyl)isoxazoles derivatives (**TTI-14**) in good to moderate yield.

4.1.3. Synthesis of 3-(7-phenylpyrazolo[1,5-*a*]pyrimidin-3-yl)-5-(thiophen-2-yl)-4-(trifluoromethyl)isoxazole. Synthesis of 3-(7-phenylpyrazolo[1,5-*a*]pyrimidin-3-yl)-5-(thiophen-2-yl)-4-(trifluoromethyl)isoxazole (**TTI-15**) was done by five step process.

Step-1: A mixture of *N,N*-dimethylformamide dimethyl acetal (10 mmol, 1 equiv.) and acetophenone **7** (10 mmol, 1 equiv.) was taken in a dry round-bottomed flask (RBF) and the reaction mixture was refluxed at 120 °C for 6 h. Then the reaction mixture was cooled to room temperature. Upon the addition of hexane to the reaction mixture at room temperature, a solid precipitate of the desired product formed. After filtration, the solid ppt was dried and used for the next step without any further purification.

Step-2: A mixture of 1*H*-pyrazol-5-amine **9** (10 mmol, 1 equiv.) and enones (10 mmol, 1 equiv.) in AcOH (5 mL) was taken in a dry round-bottomed flask (RBF) and refluxed in an oil bath. After the completion of the reaction, the resulting



solution was extracted with ethyl acetate thrice (3×10 mL), and the combined organic layer was washed with water (3×10 mL). The organic layer was dried with anhydrous Na_2SO_4 , and the solvent was evaporated under reduced pressure to afford the crude product, which was purified by column chromatography to afford 7-phenylpyrazolo[1,5-*a*]pyrimidine **10**.

Step-3: 7-Phenylpyrazolo[1,5-*a*]pyrimidine **10** (10 mmol, 1 equiv.) was taken in a round-bottom flask. DMF was added to the reaction mixture at room temperature, followed by the addition of POCl_3 (20 mmol, 2 equiv.). The progress of the reaction was monitored by TLC. After the completion of the reaction, the resulting reaction mixture was quenched with NaHCO_3 solution and then extracted with ethyl acetate thrice (3×10 mL), and the combined organic layer was washed with water (3×10 mL). The organic layer was dried with anhydrous Na_2SO_4 , and the solvent was evaporated under reduced pressure to afford the crude product, which was purified by column chromatography (5% EtOAc in hexane) to afford 7-phenylpyrazolo[1,5-*a*]pyrimidine-3-carbaldehyde **11**.

Step-4: To a solution of 1-(thiophen-2-yl)ethan-1-one **2a** (10 mmol, 1 equiv.) in ethanol water mixture (4:1) (20 mL), added an aqueous solution of NaOH (4 equiv.) followed by 7-phenylpyrazolo[1,5-*a*]pyrimidine-3-carbaldehyde **11** (10 mmol, 1 equiv.). The mixture was stirred at a low temperature for five hours, and the progress of the reaction was monitored by TLC. Then, the resulting solution was extracted with ethyl acetate thrice (3×10 mL), and the combined organic layer was washed with water (3×10 mL). The organic layer was dried with anhydrous Na_2SO_4 , and the solvent was evaporated under reduced pressure to afford the crude product, which was purified by column chromatography to afford (*E*)-3-(7-phenylpyrazolo[1,5-*a*]pyrimidin-3-yl)-1-(thiophen-2-yl)prop-2-en-1-one **12** in a quantitative yield.

Step-5: Freshly synthesized (*E*)-3-(7-phenylpyrazolo[1,5-*a*]pyrimidin-3-yl)-1-(thiophen-2-yl)prop-2-en-1-one **12** (0.5 mmol, 1 equiv.) and $\text{CF}_3\text{SO}_2\text{Na}$ (3 equiv.) were taken in an oven-dried 10 mL sealed tube, and DMSO (1.25 mL, 0.4 M) was added to that mixture. Then TBN (4 equiv.) was added to the reaction mixture, and it was stirred at room temperature. The progress of the reaction was monitored by TLC, then the sealed tube was closed very tightly and sealed properly, and the reaction mixture was heated at 120°C in an oil bath for 30 min. Then the resulting solution was extracted with ethyl acetate thrice (3×10 mL), and the combined organic layer was washed with water (3×10 mL). The organic layer was dried with anhydrous Na_2SO_4 , and the solvent was evaporated under reduced pressure to afford the crude product, which was purified by column chromatography to afford 3-(7-phenylpyrazolo[1,5-*a*]pyrimidin-3-yl)-5-(thiophen-2-yl)-4-(trifluoromethyl)isoxazole (**TTI-15**) in good to moderate yield.

4.2. General information for biology

The human breast cancer (MCF-7), prostatic small cell carcinoma (PC-3), human embryonic kidney cell line (HEK-

293), and murine mammary carcinoma cell line (4T1) were all provided by the National Center for Cell Science (NCCS, Pune, India). MCF-7, PC-3, 4T1, and HEK-293 cells were cultured using Dulbecco's modified Eagle medium (DMEM) (Himedia Laboratories Pvt. Ltd., Mumbai, India). All the cell lines have been grown in DMEM, which was enriched with 1% antibiotic (Pen strep: A001) and 10% heat-inactivated fetal bovine serum (Himedia laboratories Pvt. Ltd., Mumbai, India). Cells were maintained at 37°C in a humidified atmosphere with 5% CO_2 . The cell cytotoxic studies were performed using the yellow dye 3-(4,5-dimethylthiazol-2-yl)-2,5-diphenyltetrazolium bromide [MTT].

4.2.1. Chemicals and reagents. 100 mM stock solutions of each compound was prepared in DMSO and stored at 4°C for further investigations. Propidium iodide, RNase, acridine orange, and DAPI were all provided by Sigma-Aldrich. The TACs annexin-V/FITC-PI assay kit was purchased from Biolegend and used in accordance with the kit's instructions.

4.2.2. *In vitro* cytotoxicity and cell culture studies

MTT assay. The resulting compounds IC_{50} values against various cancer cell line types and selectivity over normal human cell lines were ascertained using the MTT assay methodology. The compounds DMSO stock solutions were diluted in a suitable media to a range of concentrations. Using the serial dilution approach, dilutions from 200 μM to 0.781 μM were made with a control solution of less than 1% DMSO in the suitable conditions. Before being seeded on a sterile 96-well plate with approximately 100 μL per well and a cell density of approximately 1×10^4 cells per well, the cells were subcultured in their respective complete medium in accordance with the ATCC protocol. They were then incubated for the overnight. The next day, the medium was aspirated, and adherent cells were treated with 200 μM to 0.781 μM of the corresponding doses. After that, the cells were nurtured in the growth medium for 48 hours. Following treatment, the medium was evacuated, and 50 μL of a 5 mg mL^{-1} MTT solution in PBS was added. After that, this combination was incubated for around three hours to see if any formazan crystals were forming. After removing the MTT solution, 150 μL of DMSO was added to each well in order to dissolve the crystals that had formed. At both 570 and 650 nanometers, the absorbance was measured. GraphPad Prism™ version 8.0.1 was used to determine the percent cell viability for the IC_{50} values, and the findings were displayed as a dose-response curve.^{25–27}

Cell apoptosis. An apoptosis experiment was performed on MCF-7 cells using a TACs/annexin V kit from Biolegend, USA. In a 12-well plate with a flat bottom, MCF-7 cells were seeded at a density of 5.0×10^4 per well, and they were left to attach overnight. After media aspiration, compound **TTI-6** and **BG-45** were treated in triplicate for 48 hours in MCF-7 cells at their respective *in vitro* IC_{50} values. The cells were washed twice with ice-cold PBS before being trypsinized. Following the trypsinization process, the cells were collected, centrifuged, and the resulting cell pellet was rinsed with ice-cold PBS before being reconstituted in 100 μL of fresh annexin V reagent, which



contained 10 μL of 10 \times binding buffer, 1 μL of FITC, 10 μL of PI, and 100 μL of double-distilled water. These samples were diluted to 500 μL using 400 μL of 1 \times binding buffer after a 30-minute dark incubation period. The samples were analyzed using flow cytometry (BDaria™ III, BD Biosciences) after incubation.^{25–27}

Cell cycle analysis. Compound **TTI-6** and **BG-45**'s cell cycle was investigated by flow cytometry using the BDaria™ III, a piece of equipment made by BD Biosciences, and the data was analyzed using FlowJo software. 5.0×10^4 MCF-7 cells were seeded onto 12-well plates and incubated for the entire night. The other day, the media was aspirated, and after adding the necessary amounts of compound **TTI-6** and **BG-45** to the aspirated media, the treatment was maintained for an additional 48 hours. The sample wells were trypsinized, washed with ice-cold PBS, and collected as a cell pellet after the treatment. Following two ice-cold PBS washes, 70% ice-cold ethanol was added dropwise to the pellet to fix it. The mixture was then gently vortexed to produce a single-cell suspension. The fixed cells were kept at -20°C for the night. Following centrifugation, the samples were resuspended in 500 μL of the staining solution, which consisted of 20% w/v RNase, 2% w/v PI, and about 0.1% v/v Triton X 100 solution in PBS. After being incubated for 30 minutes at room temperature in the dark, the dissolved samples were analyzed using flow cytometry in the BDaria™ III, BD Biosciences.^{25–27}

Nuclear staining assay. Using the lead compound **TTI-6** and the reference compound **BG-45**, a nuclear staining experiment was conducted in MCF-7 cells to gauge the extent of cancer cell disintegration. After being seeded in 12-well plates with a flat bottom, MCF-7 cells were left to adhere for the entire night before being treated with the *in vitro* IC₅₀ dosages of compound **TTI-6** and **BG-45**, respectively, and 1% DMSO as a control. After treatment, the 12-well plate was incubated for 48 hours. DAPI and acridine orange were used to label the cells after they had been fixed with 4% paraformaldehyde. A laser scanning confocal microscope (LSCM) DMI8 (Leica Microsystems, Germany) set to 63 \times magnification was used to assess the level of nuclear staining. To determine the proportion of apoptosis, ImageJ was utilized. The significance was assessed using a one-way ANOVA, and GraphPad Prism™ version 8.0.1 was used to plot the graph.^{25–27}

ROS generation. The production of reactive oxygen species in MCF-7 cells was examined utilizing the 2,7-dichlorodihydrofluorescein diacetate (DCFH-DA) assay. The non-fluorescent DCFH-DA permeates the cells, where cellular esterase removes the acetyl groups, resulting in the formation of DCFH. Reactive oxygen species convert the molecule from DCFH to DCF, resulting in the emission of green light. To achieve this purpose, MCF-7 cells were cultured in 12-well plates and incubated for 24 hours, thereafter treated with IC₅₀ dosages of compound **TTI-6** and **BG-45**, followed by a further 48 hours of incubation. After incubation, the old medium was discarded, and cells were exposed to 10 μM DCFH-DA (S0033-Beyotime) as per the prescribed protocol for 10 minutes at 37 $^\circ\text{C}$ in total

darkness. The fluorescence intensity was subsequently quantified using a laser scanning confocal microscope (LSCM) DMI8 (Leica Microsystems, Germany) at 60 \times magnification, with excitation and emission wavelengths set at 485 nm and 535 nm, respectively. The fluorescence of DCF-DA in MCF-7 cells treated with **TTI-6** was evaluated against the control group (cells treated with 1% DMSO). The enhancement of fluorescence intensity was assessed relative to the control. ImageJ was utilized to determine the relative fluorescence intensity (%). One-way ANOVA was employed to assess significance, and the graph was generated using GraphPad Prism™ version 8.0.1.^{25–27}

In silico analysis. The computational study was employed on a desktop that was configured with Intel® Core™ i7 Processor and an NVidia GPU, running on Ubuntu OS.

Target identification and energy minimization. The pharmacological target was decided based on our earlier study, where we selected HER α , following literature studies from the UniProtKB database due to its efficacy in anticancer properties. The protein HER α [PDB ID: 3ERT] was selected based on resolution of 1.9 Å [<3 Å], obtained from *Homo sapiens*, and antagonism of HER α provides excellent anticancer activity, and 4-hydroxy tamoxifen is the co-crystal ligand, present at the catalytic binding pocket. Further, the energy minimization was employed with the 'Protein Preparation Workflow' application, -utilizing preprocess with filling up of missing loop using Prime, deleting waters beyond 5 Å, at the physiological pH of 7.4. Further, H-bond optimization was employed with PROPKA pH of 7.4, and clean-up and minimization were performed using the OPLS4 force field.^{11,29,30}

Receptor grid development, docking protocol validation, and ligand preparation. Following the energy minimization of the biological target HER α , the Receptor Grid Generation application of Glide protocol was utilized for the grid-based docking protocol validation, inputting partial charges and selecting the co-crystal ligand. The grid allows the calculation at the catalytic binding pocket by removing the co-crystal ligand to develop room for other ligands for the calculation of binding affinity towards that target. The docking protocol was validated internally by docking the co-crystal ligand in an extra precision (XP) module, and superimposition provides the RMSD of the binding pose. If the RMSD is less than 2 Å, then the docking protocol was validated, as reported in the earlier studies. Further, the hit compounds from the biological studies – **TTI-3**, **TTI-5**, **TTI-6**, and **TTI-14**, along with the lead compound from our earlier study, - compound **TTI-4**, were utilized for the energy minimization protocol using LigPrep by generating possible states at the pH of 7.4, using the Epik tool for desalting, and generating tautomers, and determining the chiralities from 3D structure at 1 per ligand using OPLS4 force field.^{29–31}

Receptor–ligand docking and free binding energy MMGBSA analysis. The ligand–receptor Glide docking was carried out with compounds – **TTI-3**, **TTI-5**, **TTI-6**, **TTI-14**, and **TTI-4** using the XP module and the generated grid on the HER α , inputting the partial charges in the flexible ligand sampling, adding Epik state penalties to the docking score keeping no



constrain, and computing RMSD to input ligands. Following the molecular docking analysis for binding affinity, the free binding energy landscape was analyzed with the MMGBSA ΔG calculation of the docked binding poses. The best compound will be utilized for induced fit binding analysis to revalidate the binding protocol and eradicate the false positives.^{31,32}

Induced fit docking and molecular dynamics simulation. Compound **TTI-6** was employed for the induced fit protocol, which uses the protein and ligand flexibly by combining Prime and Glide. This protocol utilized Glide twice for initial docking and final re-docking for the conformational changes. However, Prime was employed to refine the protein–ligand complex to provide more realistic outcomes. For comparison, Compound **TTI-4** was also employed for the IFD analysis. The study was performed with extended sampling, taking the XP docking pose, taking Glide docking parameters (HER α van der Waals scaling at 0.50, ligand van der Waals scaling of 0.50, and a maximum number of poses to 80), with the Prime refinement of residues within 5 Å of ligand poses, re-docking precision of XP.^{31,32}

Further, the molecular dynamics simulation was performed with the ligand–receptor complex of compound **TTI-6**–HER α and **TTI-4**–HER α [for comparison] using the *Desmond* application of the Schrodinger suite. The study was performed using the earlier study protocol, a three-step process – system building, minimization, and MD simulation. The system building was carried out on a 5 Å orthorhombic box, neutralized by adding Na⁺ ions at a predefined SPC model, and further minimization was carried out on 100 ps. Finally, the simulation utilized the OPLS4 force field to run at NPT (300 K, 1.013 bar) for 100 ns.^{30,33}

ADMET analysis. The target binding affinity and selectivity can be observed with receptor-based *in silico* analysis using molecular docking, MMGBSA, induced fit docking, and MD simulation. Although the lead molecule is druggable or not, it could not be evaluated using the receptor-based binding analysis protocol. Therefore, the rule of five analysis for drug-likeness and other pharmacokinetic and ADME properties (QPlogP, QPlogS, BBB penetration, *etc.*) was analyzed using the QikProp tool of Maestro, along with toxicity of the lead compound **TTI-6** and compound **TTI-4** (comparison) were analyzed by pkCSM open server utilizing various descriptors.^{34,35} Further, *in silico* SAR analysis was also provided to understand the relationship between HER α –**TTI6** as anti-cancer therapeutics.

Conclusions

In conclusion, we designed a new series of synthetically challenging but highly potent class of molecules, *i.e.*, 5-(thiophen-2-yl)-4-(trifluoromethyl)isoxazoles (**TTI**) in search of novel anti-breast cancer agents. The designed molecules were directly synthesized with high yield and purity from readily available α,β -unsaturated ketones by utilizing our in-house developed sustainable synthetic strategy. The newly

synthesized molecules were properly characterized by ¹H, ¹³C, and ¹⁹F NMR and HRMS analysis and then subjected to *in vitro* screening against various cancer cell lines. These molecules were found to be more cytotoxic against human breast cancer cell lines (MCF-7), among others. The *in vitro* screening revealed a new molecule, *i.e.*, **TTI-6** (IC₅₀ = 1.91 μ M against MCF-7), as the best anti-breast cancer agent among all. Further studies, such as apoptosis induction, cell cycle analysis, and nuclear staining with **TTI-6**, suggested an apoptotic cell death mechanism. The *in silico* molecular docking, induced fit analysis, molecular dynamics simulations, and ADMET studies further supported the effects of various functional groups of **TTIs** on their anti-breast cancer activity by inhibiting the estrogen receptor alpha (ER α). Further exploration of the biodistribution and therapeutic efficacy of lead **TTI-6** *in vivo* holds significant promise, positioning it as a potential candidate for anticancer therapy.

Data availability

The data supporting this article have been included as part of the ESI.†

Author contributions

Paramita Pattanayak: methodology, investigation, data curation and writing – original draft for the chemistry part of the manuscript. Sripathi Nikhitha: methodology, investigation, data curation, and writing – original draft for the biology part of the manuscript. Debojyoti Halder: methodology, writing – original draft for the *in silico* part, software, validation. Balaram Ghosh: supervision, visualization, funding acquisition, and writing – review & editing for the biology part of the manuscript. Tanmay Chatterjee: conceptualization, supervision, visualization, project administration, funding acquisition, and writing – review & editing for the chemistry part of the manuscript.

Conflicts of interest

There are no conflicts to declare.

Acknowledgements

Dr. Tanmay Chatterjee gratefully acknowledges the Science and Engineering Research Board (SERB), Govt. India for the financial support as core research grant (SERB-CRG) (File No. CRG/2023/003045) and also the funding (File No. 02/0390/21/EMR-II) from the Council of Scientific and Industrial Research (CSIR), Govt. of India for this work. This research has also been supported by the research fund from the Department of Health Research (DHR-Indian Council of Medical Research) (File No. 11013_33_2021-GIA HR), Govt. of India and Indian Council of Medical Research (File No. 5/4-4/3/MH/2022-NCD-II) Govt. of India, provided to Dr Balaram Ghosh. The NMR facility at the BITS-Pilani, Hyderabad campus, and the HRMS facility, funded by DST-FIST (Grant



number: SR/FST/CS-I/2020/158), at BITS-Pilani, Hyderabad campus, are acknowledged. Paramita acknowledges BITS Pilani, Hyderabad Campus for her fellowship. The authors are thankful to the High-Performance Computing (HPC) facility at BITS Pilani-Hyderabad Campus for providing access to run Schrödinger Suite for *in silico* studies.

Notes and references

- D. Hanahan and R. A. Weinberg, Hallmarks of Cancer: The Next Generation, *Cell*, 2011, **144**, 646–674.
- B. Vogelstein, N. Papadopoulos, V. E. Velculescu, S. Zhou, L. A. Diaz Jr. and K. W. Kinzler, Cancer genome landscapes, *Science*, 2013, **339**(6127), 1546–1558.
- A. P. Feinberg and B. Tycko, The history of cancer epigenetics, *Nat. Rev. Cancer*, 2004, **4**, 143–153.
- S. B. Baylin and P. A. Jones, A decade of exploring the cancer epigenome—biological and translational implications, *Nat. Rev. Cancer*, 2011, **11**, 726–734.
- C. J. Sherr, Cancer cell cycles, *Science*, 1996, **274**(5293), 1672–1677.
- M. Esteller, Epigenetics in cancer, *N. Engl. J. Med.*, 2008, **358**(11), 1148–1159.
- N. Harbeck and M. Gnant, Breast cancer, *Lancet*, 2017, **389**(10074), 1134–1150.
- K. Polyak, Heterogeneity in breast cancer, *J. Clin. Invest.*, 2011, **121**(10), 3786–3788.
- A. G. Rivenbark, S. M. O'Connor and W. B. Coleman, Molecular and cellular heterogeneity in breast cancer: challenges for personalized medicine, *Am. J. Pathol.*, 2013, **183**(4), 1113–1124.
- S. Ali and R. C. Coombes, Estrogen Receptor Alpha in Human Breast Cancer: Occurrence and Significance, *J. Mammary Gland Biol. Neoplasia*, 2000, **5**(3), 271–281.
- A. K. Shiau, D. Barstad, P. M. Loria, L. Cheng, P. J. Kushner, D. A. Agard and G. L. Greene, The Structural Basis of Estrogen Receptor/Coactivator Recognition and the Antagonism of This Interaction by Tamoxifen, *Cell*, 1998, **95**, 927–937.
- R. S. Keri, A. Hiremathad, S. Budagumpi and S. A. Patil, Isoxazole and its biological activities: A review, *Eur. J. Med. Chem.*, 2014, **78**, 340–374.
- Y. Wang, Y. Zhang, Z. Yang and H. Guo, Synthesis and biological evaluation of isoxazole derivatives as anticancer agents, *Bioorg. Chem.*, 2021, **112**, 104898.
- R. B. De Oliveira and S. J. Garden, Isoxazole derivatives as potential anti-inflammatory agents, *Curr. Med. Chem.*, 2002, **9**(11), 1095–1121.
- N. Agrawal and P. Mishra, The synthetic and therapeutic expedition of isoxazole and its analogues, *Med. Chem. Res.*, 2018, **27**, 1309–1344.
- J. Zhua, J. Moa, H.-z. Lina, Y. Chenb and H. p. Suna, The recent progress of isoxazole in medicinal chemistry, *Bioorg. Med. Chem.*, 2018, **26**, 3065–3075.
- Y. Narayan, A. Kumar and A. Parveen, “Thiophene”: A Sulphur Containing Heterocycle as a Privileged Scaffold, *Lett. Drug Des. Discovery*, 2024, **21**(11), 1922–1935.
- S. Thakur, D. Kumar, S. Jaiswal, K. K. Goel, P. Rawat, V. Srivastava, S. Dhiman, H. R. Jadhav and A. R. Dwivedi, Medicinal chemistry-based perspectives on thiophene and its derivatives: exploring structural insights to discover plausible druggable leads, *RSC Med. Chem.*, 2025, **16**, 481.
- S. P. Archana and P. A. Chawla, Thiophene-based derivatives as anticancer agents: An overview of a decade's work, *Bioorg. Chem.*, 2020, **101**, 104026.
- G. Martinez, K. Tolentino, P. Sukheja, J. Webb, C. W. McNamara, A. K. Chatterjee and B. Yang, Novel isoxazole thiophene-containing compounds active against Mycobacterium tuberculosis, *Bioorg. Med. Chem. Lett.*, 2025, **119**, 130108.
- P. Paramita, S. Nikhitha, D. Halder, B. Ghosh and T. Chatterjee, Exploring the impact of trifluoromethyl (–CF₃) functional group on the anti-cancer activity of isoxazole-based molecules: design, synthesis, biological evaluation and molecular docking analysis, *RSC Adv.*, 2024, **14**, 18856–18870.
- P. Pattanayak and T. Chatterjee, Synthesis of (4-Trifluoromethyl)isoxazoles through a Tandem Trifluoromethyloximation/Cyclization/Elimination Reaction of α,β -Unsaturated Carbonyls, *J. Org. Chem.*, 2023, **88**, 5420–5430.
- M. M. Hammouda, H. E. Gafferc and K. M. Elattar, Insights into the medicinal chemistry of heterocycles integrated with a pyrazolo[1,5-a]pyrimidine scaffold, *RSC Med. Chem.*, 2022, **13**, 1150.
- S. Cherukupalli, R. Karpoormath, B. Chandrasekaran, G. A. Hampannavar, N. Thapliyal and V. N. Palakollu, An insight on synthetic and medicinal aspects of pyrazolo[1,5-a]pyrimidine scaffold, *Eur. J. Med. Chem.*, 2017, **126**, 298e352.
- S. Pulya, A. Himaja, M. Paul, N. Adhikari, S. Banerjee, G. Routholla, S. Biswas, T. Jha and B. Ghosh, Selective HDAC3 Inhibitors with Potent *In Vivo* Antitumor Efficacy against Triple-Negative Breast Cancer, *J. Med. Chem.*, 2023, **66**(17), 12033–12058.
- S. Pulya, T. Patel, M. Paul, N. Adhikari, S. Banerjee, G. Routholla, S. Biswas, T. Jha and B. Ghosh, Selective Inhibition of Histone Deacetylase 3 by Novel Hydrazide-Based Small Molecules as Therapeutic Intervention for the Treatment of Cancer, *Eur. J. Med. Chem.*, 2022, **238**, 114470.
- G. Routholla, S. Pulya, T. Patel, A. Sk, N. Amin, S. Adhikari, T. J. Biswas and B. Ghosh, Synthesis, Biological Evaluation, and Molecular Docking Analysis of Novel Linker-Less Benzamide-Based Potent and Selective HDAC3 Inhibitors, *Bioorg. Chem.*, 2021, **114**, 105050.
- D. Halder, S. Das, A. Ramesh and R. S. Jeyaprakash, Molecular docking and dynamics-based approach for the identification of kinase inhibitors targeting PI3K α against non-small cell lung cancer: a computational study, *RSC Adv.*, 2022, **12**, 21452–21467.
- Schrödinger Release 2025-1: Protein Preparation Workflow; *Epik*, Schrödinger, LLC, New York, NY, 2024; *Impact*, Schrödinger, LLC, New York, NY; *Prime*, Schrödinger, LLC, New York, NY, 2025.



- 30 C. Lu, C. Wu, D. Ghoreishi, W. Chen, L. Wang, W. Damm, G. A. Ross, M. K. Dahlgren, E. Russell, C. D. Von Bargen, R. Abel, R. A. Friesner and E. D. Harder, OPLS4: Improving Force Field Accuracy on Challenging Regimes of Chemical Space, *J. Chem. Theory Comput.*, 2021, **17**, 4291–4300.
- 31 D. Halder, R. S. Jeyaparakash and B. Ghosh, A Structure-Based Design Strategy with Pyrazole-Pyridine Derivatives Targeting TNF α as Anti-Inflammatory Agents: E-Pharmacophore, Dynamic Simulation, Synthesis and *In Vitro* Evaluation, *Chem. Biodiversity*, 2024, **21**(9), DOI: [10.1002/cbdv.202400778](https://doi.org/10.1002/cbdv.202400778).
- 32 *Schrödinger Release 2023-1: Glide*, Schrödinger, LLC, New York, NY, 2021.
- 33 *Schrödinger Release 2021-4: Desmond Molecular Dynamics System*, D. E. Shaw Research, New York, NY, 2021; *Maestro-Desmond Interoperability Tools*, Schrödinger, New York, NY, 2021.
- 34 *Schrödinger Release 2023-3: QikProp*, Schrödinger, LLC, New York, NY, 2023.
- 35 D. E. V. Pires, T. L. Blundell and D. B. Ascher, pkCSM: Predicting Small-Molecule Pharmacokinetic and Toxicity Properties Using Graph-Based Signatures, *J. Med. Chem.*, 2015, **58**, 4066–4072.

